

Modelling the adsorption of fluoride onto activated alumina in the presence of other ions

Naga Samrat MVV, Gandhi K S, Kesava Rao K*

Department of Chemical Engineering, Indian Institute of Science, Bengaluru 560012, India

Abstract

Most of the studies on the adsorption of F^- are experimental, and have been done with synthetic solutions. Such studies rarely mimic the field situation. Therefore, selection of an adsorbent that can remove F^- from any kind of feed requires models that can predict the adsorption behavior for any given set of input conditions. From our observations and as also reported by many authors, the adsorption of F^- is affected by the presence of many ions. When modelling the adsorption of F^- , it is usually taken as a single entity getting adsorbed on the adsorbent. As this is not a proper assumption, a model was developed which takes into account all the speciation reactions that take place during adsorption, and all the species like H^+ , OH^- , Na^+ , Cl^- , and NO_3^- present in the solution along with F^- . As an electrolyte system is involved, the Nernst-Planck equations were used to obtain the flux of each species. Using the model, the equilibrium constants and rate constants for the reactions were obtained. For one initial concentration of F^- , a reasonable fit was obtained to the batch adsorption data, except at short times. Because of an uncertainty in the amount of impurity present in the commercial adsorbent used, there was a significant discrepancy between predictions and data at higher initial concentrations of F^- . The present model can be applied to any charged adsorbent.

Keywords: Activated alumina; batch adsorption; defluoridation; Nernst-Planck equations;

*Corresponding author

Email address: kesava@chemeng.iisc.ernet.in (Kesava Rao K)

1. Introduction

Most of the studies on adsorption of F^- are experimental, and have been done with synthetic solutions. Such studies rarely mimic the field situation. Therefore, selection of an adsorbent that can remove F^- from any kind of feed requires models that can predict the adsorption behavior for any given set of input conditions. Data on most of the adsorbents used for the adsorption of F^- are observed to agree well with Langmuir or Freundlich isotherms (Mondal and George, 2015). In the context of kinetics, they are fitted either to Langmuir kinetics, pseudo-first-order or pseudo-second-order kinetics. With the use of an analytical or numerical solution, we can predict the performance of the adsorbent without the need for laborious experiments.

In the light of the above observations, the motivation for the present work is as follows. Many papers show that the presence of an another ion along with F^- influences the adsorption of F^- (Nigussie et al., 2007; Goswami and Purkait, 2012; Chatterjee and De, 2014). However, with respect to modelling the adsorption of F^- , there are about 2 to 3 other ions always present in water. These ions often affect the structural properties of the adsorbent (Okamoto and Imanaka, 1988; Su and Suarez, 1997; Al-Abadleh and Grassian, 2003) and very few theoretical studies exist on the combined effect of multiple ions on the adsorption of F^- . Most of the available models do not account for the presence of other ions. Therefore, here a model has been developed to predict the adsorption behaviour of F^- in the presence of H^+ , OH^- , Cl^- , NO_3^- , and Na^+ .

In the papers of Fletcher et al. (2006) and Tang et al. (2009), the concentration of H^+ is taken as an independent variable. Hao and Huang (1986) assume that the surface concentration of H^+ depends on the electric potential of the surface, as the alumina surface becomes charged in solution. It is also assumed that the equilibrium constants depend on the pH of the solution (Hao and Huang, 1986; Fletcher et al., 2006). In the present work, the pH is permitted to change with time, and the complexity arising because of the surface potential is neglected.

2. Materials and methods

2.1. Experimental setup

Adsorption was studied in the batch mode. Two setups were used. In one setup, a conical flask containing 200 mL of solution and 1 g of activated

Table 1: Characteristics of AA pellets of grade OAS37, as provided by the manufacturer Oxide (India) Catalysts Pvt. Ltd., Durgapur, India and experimentally measured.

Property	Quantity	
	Manufacturer	Experimental
bulk density (kg/m^3)	880	786
surface area (m^2/g)	200	170
porosity	0.2	0.33
loss on attrition (%)	0.10	—
Al_2O_3 (weight %)	93.74	—
Fe_2O_3 (weight %)	0.05	—
SiO_2 (weight %)	0.20	—
Na_2O (weight %)	0.35	—
loss on ignition (at 900°C) (weight %)	5.66	—

alumina adsorbent was used. The details of the adsorbent are given in Table 1. The flask was placed in a rotary shaker which was rotated at a speed of 100 rpm. In these experiments, it is expected that shaking will provide good mixing and hence a uniform distribution of the solution and the adsorbent. However, the adsorbent accumulated as a stationary heap near the center of the flask even with a rotation speed of 100 rpm. Thus the relative velocity between the fluid and particles is uncertain. When the shaker speed was increased beyond 100 rpm, there was fluidization of the adsorbent pellets, but after some time of operation, attrition of the pellets occurred, leading to a reduction in their size.

In order to prevent the attrition and also to get an estimate of the relative velocity v_{ra} of the fluid with respect to adsorbent, a different experimental setup was used. The need to estimate v_{ra} arises because of the dependence of the external mass transfer coefficient on v_{ra} . Therefore, the data were acquired using a differential bed adsorber (DBA). The DBA experiments were done using a glass column of inner diameter 18 mm and the flow was controlled using a peristaltic pump (Fig. 1). The flow rate of the liquid through the DBA was maintained at 1.5 mL/s and could not be increased beyond this value owing to limitations of the available peristaltic pump. The adsorbent bed of height 1 cm was sandwiched between 5 cm beds of glass beads to ensure a uniform distribution of the fluid, especially when flow was

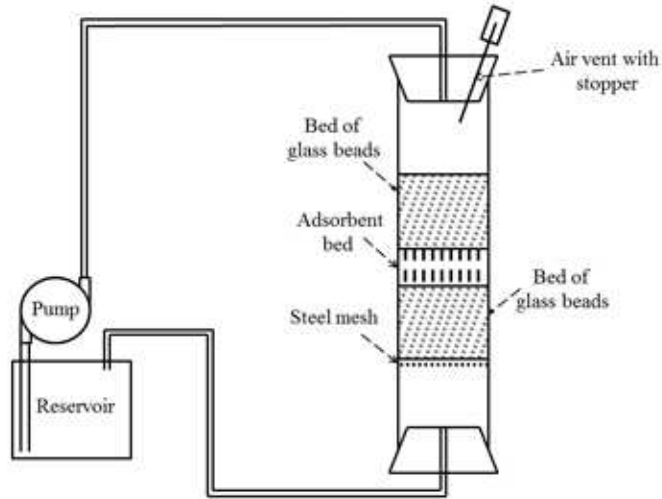


Figure 1: Schematic view of the differential bed adsorber used for the batch experiments.

from the top to the bottom. The lower bed was supported on a steel mesh, and the contents were loaded into the column after filling it with the solution of interest. This prevented the formation of air gaps in the bed, which could cause channelling of the fluid. The adsorbent height of 1 cm corresponds to a weight of 2 g and the total volume of the circulating solution was taken such that the solids concentration or bulk density was 5 g/L.

The bed porosity ϵ_b was determined by noting the change in the level of water immediately after adding the pellets. It was found that $\epsilon_b = 0.59$. Using a microscope, the diameters of about 10 particles were measured. The masses of the group of particles was measured and hence the averaged particle density ρ_p could be calculated. It was found that $\rho_p = 1910 \text{ kg/m}^3$.

Before loading into the column, the adsorbent was soaked in deionised water for 24 h. This was performed to remove any unwanted impurities that were present on the adsorbent, as the used AA was a commercial grade alumina. Adsorption of single ions onto AA was studied at first to determine the adsorption efficiency of AA towards these ions. The concentration of ions were varied from 40 mg/L to 5 mg/L for F^- , 500 mg/L to 20 mg/L for SO_4^{2-} , and 1000 mg/L to 10 mg/L for HCO_3^- . After these experiments, binary combinations of the ions (i) F^- and Cl^- , (ii) F^- and NO_3^- were used. The change in the concentrations of the ions in the solution due to

adsorption was measured by collecting samples at regular intervals of time. All the experiments were conducted at room temperature (26 - 30 °C).

2.2. Chemicals and chemical analysis

All the chemicals used in the preparation of the solutions were of analytical grade, and were used without any further purification. Deionised water having a conductivity of $0.05\ \mu\text{S}/\text{cm}$ was obtained from a Millipore unit.

Analysis of the samples was done using an ion chromatograph (Metrohm 883 Basic IC plus) for anions and cations. The 95% confidence limits were calculated using the data for the standards and the t -distribution (Snedecor and Cochran, 1968). The error bars shown in the figures correspond to these limits. In order to operate the chromatographic column below the maximum number of exchange sites available in the column, it was recommended to dilute the samples. During the analysis, the samples of ROR, SRW, and SNW were diluted 5 or 10 times and samples of SFW were used without dilution. As the bicarbonate concentration cannot be measured using this method, it was calculated using titration (Eaton et al., 2005, p. 2.27). The concentration of total carbonate comprising CO_3^{2-} , HCO_3^- , and $\text{CO}_2(\text{aq})$ was calculated from the pH of solution, the pK values of carbonic acid, and the bicarbonate concentration obtained by titration. The quality of the analysis based on the ion chromatograph was checked using international standards like ION 915, ION 96.4, and MISSIPPI - 03. It was found that the concentrations of all ions quantified were within 5% of the certified values of these standards.

2.3. Surface studies

The determination of the possible reactions that can occur on the adsorbent can be determined by a study of its surface. It is known that the surface of AA changes with time upon soaking in water (Wijnja and Schulthess, 1999; Lefevre et al., 2002; Ryazanov and Dudkin, 2004; Carrier et al., 2007). This is mainly attributed to the hydration of the alumina surface, which was observed to change to bayerite or gibbsite based on the pH of the solution (Carrier et al., 2007). As the hydration reactions involve the use of H^+ ions, the use of titration can give us an insight into the equilibrium constants of these reactions.

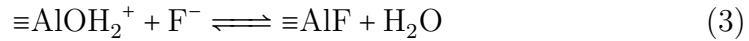
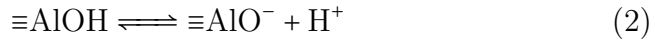
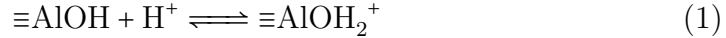
Potentiometric titration experiments were done using a Mettler Toledo auto titrator (DL50 Rondolino). This was equipped with an automatic microburet and the pH of the solution after the subsequent addition of the

titrant was measured by a Mettler Toledo pH electrode (DG111 - SC) containing 3 M KCl solution. The pH meter was calibrated using Merck standard solutions of pH 4.0 and 7.0. For all the experiments, 0.02 N HCl solution was used as the titrant. It was calibrated using 5 mL of 0.02 N tris-hydroxy methyl amino methan (TRIZMA) solution. The solution to be titrated consisted of 0.25 g of the adsorbent suspended in 10 mL of de-ionized water. This solution was made alkaline by the addition of 1 mL of 1 N NaOH, and the pH was 12.0.

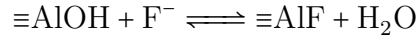
3. A model for titration and batch adsorption

A good model is needed to predict the adsorption behaviour for various concentrations of the ions. Isotherms like Langmuir, Freundlich, and Sips have been used to predict the equilibrium behaviour for the adsorption of F^- (Mondal and George, 2015), but it is assumed that there is only one species in the solution. It is also assumed that the adsorbent consists of only occupied and vacant sites. In practice, there is more than one species in the solution and there is a competition between the species for adsorption. Further, the adsorbent consists of different kinds of sites which can form varied complex species. Therefore, it is essential to include the concentrations of the other species in the model as well as different products formed by different sites. With these assumptions one can predict the equilibrium composition on the adsorbent and of the solution for any given initial condition.

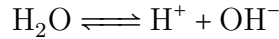
The papers which show a decreased uptake of F^- in the presence of other ions do not mention or model how the concentrations of these ions change with time (Islam and Patel, 2007; Tang et al., 2009; Dou et al., 2011; Chatterjee and De, 2014). During the adsorption process, the following reactions have been proposed (Hao and Huang, 1986)



where \equiv denotes a surface group. Here the reaction



is not considered because it can be obtained by the addition of reaction (1), (3), and the water reaction.



In the most commonly used modelling approaches (Nigussie et al., 2007; Mondal and George, 2015) only (3) has been used. From (1) - (3) it can be seen that along with the adsorbed species $\equiv\text{AlF}$, there are also $\equiv\text{AlOH}$, $\equiv\text{AlOH}_2^+$, and $\equiv\text{AlO}^-$ present on the adsorbent. So there is need to consider these species also. The groundwater usually contains many other species like HCO_3^- , SO_4^{2-} , etc. along with F^- . If there is competitive adsorption, then a few more species will also be produced (Wijnja and Schulthess, 1999; Appel et al., 2013).



In the present section, the assumptions and governing equations for the multicomponent adsorption are discussed. First, it is assumed that the charge neutrality is separately obeyed by the adsorbent and the solution. In existing models, the surface of the adsorbent is assumed to be charged, and the charge is balanced by an electrical double layer of ions in the solution (Bockris et al., 2006) (Fig. 2). The surface concentration $c_{i,s}$ and bulk concentration c_i of

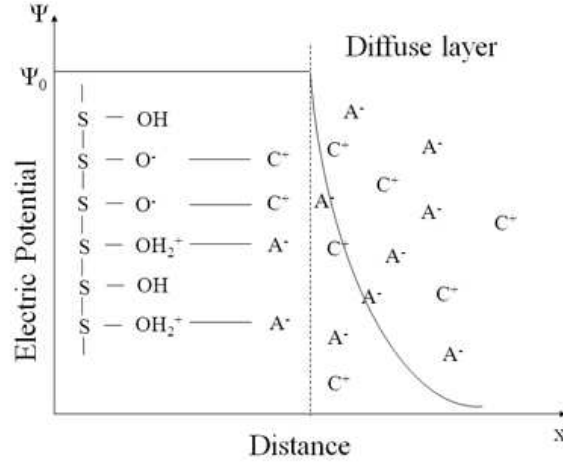


Figure 2: Schematic view of the possible distribution of the ions at the surface of a charged solid. Here C^+ and A^- denote cations and anions, respectively, and S denotes a surface site.

an ion i at equilibrium, i.e. when there is no mass transfer, are related by

$$c_{i,s} = c_i e^{\frac{-z_i F \psi_0}{RT}} \quad (6)$$

where ψ_0 is the surface potential, or potential at the outer Helmholtz plane, F is Faraday constant, R is universal gas constant, and T is the absolute temperature of the system (Hao and Huang, 1986). However, accounting for the diffuse double layer makes models of continuous contacting unwieldy. Further (6) is not strictly valid when the rate of adsorption is non-zero. The assumption of charge neutrality for the solid phase is equivalent to assuming a sharp double layer equivalent to a group of capacitors in parallel. Hence the concentrations at the surface and the bulk are assumed to be equal.

The charged species formed on the solid surface are assumed to be neutralised by non-reactive ions present in the solution. In the present study, chloride, nitrate and sodium were found to not complex with the adsorbent i.e., they were non-reactive. Similarly Nagashima and Blum (1999) found that Na^+ did not affect the adsorption of H^+ onto γ - alumina. Thus, it is assumed that $\equiv\text{AlOH}_2^+$ is neutralized by either Cl^- or NO_3^- . In the present case, the basis for taking Cl^- in a solution made from NaF and deionized (DI) water is that the pH of the DI water was about 6.0, but the water without any ions should have a pH of 7.0. Therefore, upon analysis of this DI water for anions using an ion chromatograph, it was also observed that there was a minute peak for Cl^- which is below the limit of detection (Fig. 3). Similarly,

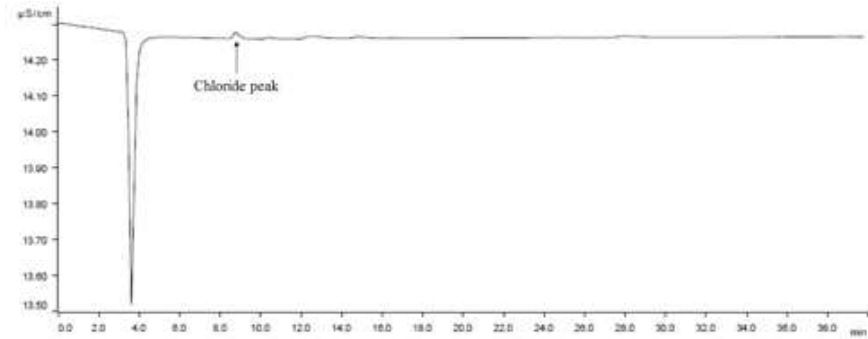
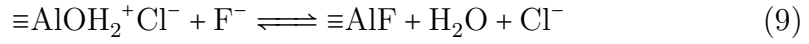


Figure 3: Chromatogram from an ion chromatograph for anions in deionized water. Here the x-axis represents the time and the y-axis represents the conductivity.

for $\equiv\text{AlO}^-$, Na^+ is the counter ion, as it is added along with F^- . Hence (1)

- (3) are replaced by



Equilibrium constants for (7) and (8) were obtained by titration, and for (9) by batch adsorption.

3.1. Titration

The reactions that occur during titration are (7) and (8) and the equilibrium constants for these reactions are given by

$$K_1 = \frac{\hat{a}_1}{\hat{a}_2 a_1} \quad (10)$$

$$K_2 = \frac{\hat{a}_3 a_1}{\hat{a}_2} \quad (11)$$

where \hat{a}_1 - \hat{a}_3 , and a_1 are the electrochemical activities (Benjamin, 2002, pg. 598) of $\equiv\text{AlOH}_2^+\text{Cl}^-$, $\equiv\text{AlOH}$, $\equiv\text{AlO}^-\text{Na}^+$, and H^+ , respectively. As the double layer is collapsed onto a single plane in our model, $\psi_0 = 0$. Hence, the electrochemical activities may be replaced by the chemical activities. Considering the adsorbed phase to be an ideal solution, the activities may be replaced by the mole fractions $\{y_i\}$ in the adsorbed phase. Similarly, considering a dilute solution $a_1 = \frac{c_1}{c_{1,0}}$ where $c_{1,0} = 1.0$ mol/L is a reference concentration. Therefore, with these assumptions (10) and (11) can be rewritten as

$$K_1 = \frac{q_1}{q_2 c_1} \quad (12)$$

$$K_2 = \frac{q_3 c_1}{q_2} \quad (13)$$

where $q_j = y_j c_T$ is the concentration of adsorbed species j (moles of j per unit mass of the adsorbent), c_T is the total number of sites on the adsorbent (moles per unit mass of the adsorbent), and c_i is the concentration of solute species i (moles of i per unit volume of the solution).

For (7) and (8), q_j with j varying from 1-3 corresponds to the species $\equiv\text{AlOH}_2^+\text{Cl}^-$, $\equiv\text{AlOH}$, $\equiv\text{AlO}^-\text{Na}^+$, respectively, and c_1 corresponds to the

concentration of H^+ in the solution. The expressions for the equilibrium equations (12) and (13) are consistent with simple mass action kinetics for the special case where the charge-neutralising counter ions do not participate in the adsorption or complexing process. Neutralisation occurs just based on Coulombic attraction. Similar mass action kinetics were found suitable by Winkler and Thodos (1971) for the removal of phosphate by activated alumina activated with HNO_3 , where the measured rate was independent of the concentration of nitrate in the solution.

In the titration experiment, the titrant was HCl and the solution to be titrated consisted of AA in $NaOH$. The mass balances for Cl^- and Na^+ are given by

$$c_{3i}V_a + c_{imp}V_a = c_3(V_a + V_b) + m_p q_1 \quad (14)$$

$$c_{5i}V_b = c_5(V_a + V_b) + m_p q_3 \quad (15)$$

where c_3 and c_5 are the concentrations of Cl^- and Na^+ , respectively, c_{3i} is the concentration of the titrant (acid), c_{5i} is the initial concentration of the base, V_b is the volume of the base taken, V_a is the volume of the acid added, m_p is the mass of the adsorbent taken, and c_{imp} is the total concentration of impurity present in the solution after addition of the acid. As mentioned earlier, the AA used in the experiments was a commercial adsorbent which contained some impurities. In view of the leaching of NO_3^- from the fresh adsorbent when it is soaked in deionized water, it was assumed that the impurity was NO_3^- . The term $c_{imp}V_a$ represents an ad hoc attempt to include the leaching of nitrate into the solution during titration. More satisfactory alternatives will be explored in the future. As shown later, there was no adsorption of Cl^- and NO_3^- on the adsorbent. Also, because of the same charge of these ions, Cl^- and NO_3^- are treated interchangeably in modelling. In addition, the solution must be electrically neutral, or

$$c_1 - c_3 - \frac{K_w}{c_1} + c_5 = 0 \quad (16)$$

Here c_1 is the concentration of H^+ and K_w is ionic product of water. In (16), K_w/c_1 gives the concentration of OH^- in solution. There can be a loss of aluminium in the form of soluble complexes such as $AlF_n(H_2O)_{6-n}^{(3-n)}$, AlF_n^{3-n} , and $AlOH_n^{3-n}$ (Nordin et al., 1999; George et al., 2010; Jin et al., 2010). This factor has been ignored in the present work.

The mass balance for the adsorbates is given by

$$q_1 + q_2 + q_3 = c_T \quad (17)$$

where q_i are the concentrations of species on the adsorbent. There are six equations (12) - (17) and seven unknowns c_1 , c_3 , c_5 , q_1 , q_2 , q_3 , and V_a . Therefore, in order to obtain a unique solution, we need to specify one of the seven unknowns. In the titration experiment, the pH of the solution is measured as a function of the volume of the titrant added V_a . Equations (12) to (17) can be solved to obtain V_a in terms of c_1 as

$$V_a = \frac{\left(c_{5i} + c_1 - \frac{K_w}{c_1}\right) V_b + \left(1 - \frac{K_2}{K_1 c_1^2}\right) \frac{m_p c_T}{1 + \frac{1}{K_1 c_1} + \frac{K_2}{K_1 c_1^2}}}{c_{3i} + c_{imp} - \left(c_1 - \frac{K_w}{c_1}\right)} \quad (18)$$

The above equation can be rewritten in terms of the pH as

$$V_a = \frac{\left(c_{5i} + 10^{-pH} - \frac{K_w}{10^{-pH}}\right) V_b + \left(1 - \frac{K_2}{K_1 10^{-2pH}}\right) \frac{m_p c_T}{1 + \frac{1}{K_1 10^{-pH}} + \frac{K_2}{K_1 10^{-2pH}}}}{c_{3i} + c_{imp} - \left(10^{-pH} - \frac{K_w}{10^{-pH}}\right)} \quad (19)$$

Equation (19) can be used to estimate the values of K_1 , K_2 , c_T , and c_{imp} by fitting it to the data of pH vs. V_a .

3.2. Batch adsorption: equilibrium

The above methodology can be followed for relating the variables involved in the batch adsorption of F^- . An equation for the mass balance of F^- has to be added, and the other mass balances have to be modified as titrant is not added to the solution. Equations (14) - (15) are modified to

$$c_{2i} = c_2 + \rho_b q_4 \quad (20)$$

$$c_{3i} + \rho_b q_{1i} = c_3 + \rho_b q_1 \quad (21)$$

$$c_{5i} = c_5 + \rho_b q_3 \quad (22)$$

where c_2 and q_4 are the concentrations of F^- and $\equiv AlF$, respectively, and ρ_b is the mass of adsorbent pellets per unit volume of the solution in the bed and

the stirred vessel (Fig. 4). Here the mass balance for Cl^- is changed because during the batch experiments, the adsorbent was taken after soaking in DI water for 24 h and the solution which contained the leachate was discarded, whereas the titration experiments were done along with the leachate. Here q_{1i} is the initial concentration of the impurity/leachate present on the adsorbent. The equilibrium constant for the reaction (9) is defined as

$$K_3 = \frac{q_4}{q_1 c_2} \quad (23)$$

The charge neutrality equation for the solution is

$$c_1 - c_2 - c_3 - \frac{K_w}{c_1} + c_5 = 0 \quad (24)$$

Therefore, there are eight unknowns $c_1, c_2, c_3, c_4, q_1, q_2, q_3, q_4$ and eight equations (12, 13, 20 - 24).

3.3. Batch adsorption: kinetics

Till now, the equations governing equilibrium were discussed. Modelling batch adsorption or continuous processing in a column requires rate data, in addition to equilibrium data. The setup shown in Fig. 1 was used to obtain data on adsorption kinetics, and the notation for the concentrations is shown in Fig. 4. The volume of the adsorber bed is very small compared to the volume of the stirred vessel.

For convenience, the species in the solution are numbered such that 1 denotes H^+ , $n - 1$ denotes OH^- , and n denotes any species whose concentration is eliminated using the electroneutrality condition. For example, for a 5-species system containing H^+ , Cl^- , OH^- , F^- , and Na^+ , we have $1 = \text{H}^+$, $2 = \text{F}^-$, $3 = \text{Cl}^-$, $4 = \text{OH}^-$, and $5 = \text{Na}^+$. One of the important variables is the pH. As it affects the adsorption of F^- , special effort was made to account for the changes in pH, by treating the reaction between H^+ and OH^- as instantaneous.

The mass balance for species i in a well-mixed stirred vessel is given by

$$V \frac{dc_i}{dt} = \dot{Q}(c_{i,f} - c_i) + V \dot{R}_i; \quad i = 1, n \quad (25)$$

where V is the volume of the liquid in the vessel, $c_{i,f}$ and c_i are the inlet and outlet concentrations, respectively, \dot{Q} is the volumetric flowrate of the liquid,

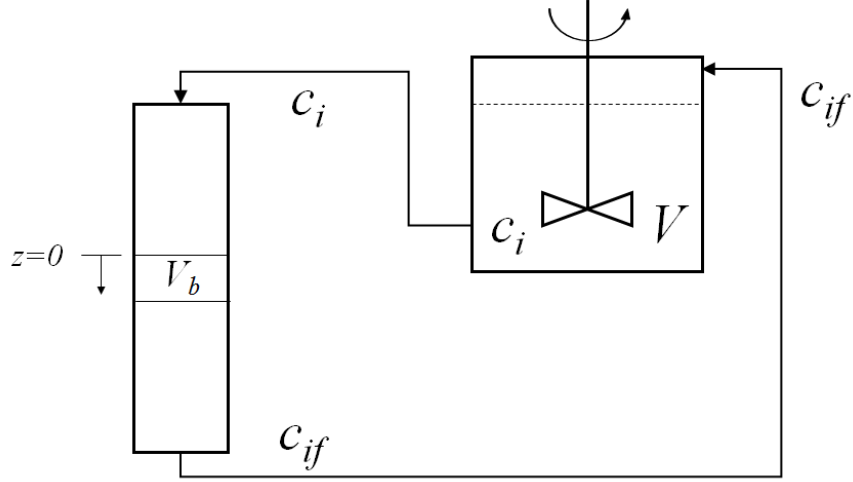


Figure 4: Sketch of the differential adsorber used for the batch experiments.

and \dot{R}_i is the molar rate of production of i per unit volume by chemical reactions. We have

$$\dot{R}_i = 0; \quad i \neq 1 \text{ \& } n-1 \quad (26)$$

$$\dot{R}_1 = \dot{R}_{n-1} = k_f c_{\text{H}_2\text{O}} - k_b c_{\text{H}^+} c_{\text{OH}^-} \quad (27)$$

where k_f and k_b are the rate constants for the reaction



It is assumed that (28) is always close to equilibrium. Hence $\dot{R}_1 \approx 0$ and

$$K_w = \frac{a_{\text{H}^+} a_{\text{OH}^-}}{a_{\text{H}_2\text{O}}} \approx c_{\text{H}^+} c_{\text{OH}^-} \quad (29)$$

where a_i is the activity of species i and c_{H^+} is the concentration of H^+ in mol/L. Hence, $c_{\text{OH}^-} = c_{n-1} = K_w/c_1$. To eliminate \dot{R}_1 , we subtract the mass balance for $i = n-1$ from the balance for $i = 1$ to obtain

$$V \left(\frac{dc_1}{dt} - \frac{dc_{n-1}}{dt} \right) = \dot{Q} [(c_{1,f} - c_1) - (c_{n-1,f} - c_{n-1})] \quad (30)$$

In (30), c_{n-1} is replaced by K_w/c_1 .

The charge neutrality condition is used to eliminate the concentration of the n^{th} species. Thus

$$\sum_{i=1}^n z_i c_i = 0 \Rightarrow c_n = - \sum_{i=1}^{n-1} \frac{z_i c_i}{z_n} \quad (31)$$

where z_i is the charge of species i , expressed in multiples of the charge of the electron. Using (29) and noting that $z_1 = 1$, and $z_{n-1} = -1$, (31) reduces to

$$c_n = -\frac{1}{z_n} \left(c_1 - \frac{K_w}{c_1} \right) - \sum_{i=2}^{n-2} \frac{z_i}{z_n} c_i \quad (32)$$

Therefore, it is necessary to solve only $n - 1$ mass balances, and c_n can be obtained from (32). Hence the mass balances for species i in the stirred vessel are given by

$$V \frac{d}{dt} \left(c_1 - \frac{K_w}{c_1} \right) = \dot{Q} \left[(c_{1,f} - c_1) - \left(\frac{K_w}{c_{1,f}} - \frac{K_w}{c_1} \right) \right] \quad (33)$$

$$V \frac{dc_i}{dt} = \dot{Q}(c_{i,f} - c_i); \quad i = 2, n-2 \quad (34)$$

Let us now consider the model for the differential packed bed. The external mass transfer rate to each pellet is calculated using a film model with the assumption that a liquid film of thickness δ surrounds the pellet. As is customary, convection and accumulation are neglected in the film. The dissociation of water is instantaneous and is permitted to occur in the film. The other reactions need adsorbent and occur only in the pellets. As before, the solution is assumed to remain electrically neutral. The film thickness is assumed to be small compared to the particle size, and the curvature of the film is neglected. Let \tilde{N}_{ix} denote the molar flux of i in the x-direction (negative radial direction) (Fig. 5). The mass balance for species i in the bulk liquid is given by

$$\frac{\partial}{\partial t}(\epsilon_b c_{i,b}) + \frac{\partial}{\partial z} N_{i,z} = -a_p \tilde{N}_{i,x}|_{x=0} + \dot{R}_{i,b}; \quad i = 1, n \quad (35)$$

where \dot{R}_{ib} is the molar rate of production of i per unit volume of the bed, ϵ_b is the porosity of the bed, and $a_p = 3(1 - \epsilon_b)/R_p$ is the external surface area of the pellets per unit volume of the bed. As in the case of the stirred vessel,

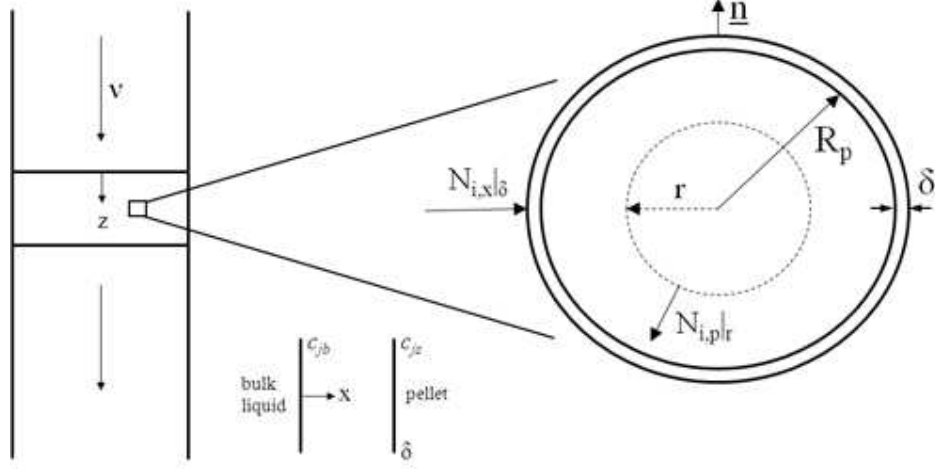


Figure 5: Sketch of the different fluxes into the pellet and the liquid film surrounding it. Here R_p is the radius of the pellet, and \underline{n} is the unit outward normal to the external surface of the pellet.

in the bulk liquid, we have

$$\dot{R}_{i,b} = 0; \quad i \neq 1 \text{ \& } n-1 \quad (36)$$

$$\dot{R}_{1,b} = \dot{R}_{n-1,b} = k_f c_{\text{H}_2\text{O}} - k_b c_{\text{H}^+} c_{\text{OH}^-} \quad (37)$$

Proceeding as in the case of the stirred vessel, we obtain

$$\frac{\partial}{\partial t} \left[\epsilon_b \left(c_{1,b} - \frac{K_w}{c_{1,b}} \right) \right] + \frac{\partial}{\partial z} [N_{1,z} - N_{n-1,z}] = -a_p [\tilde{N}_{1,x} - \tilde{N}_{n-1,x}]|_{x=0} \quad (38)$$

$$\frac{\partial}{\partial t} (\epsilon_b c_{i,b}) + \frac{\partial}{\partial z} N_{i,z} = -a_p \tilde{N}_{i,x}|_{x=0}; \quad i = 2, n-2 \quad (39)$$

$$c_{n,b} = -\frac{1}{z_n} \left(c_{1,b} - \frac{K_w}{c_{1,b}} \right) - \sum_{i=2}^{n-2} \frac{z_i}{z_n} c_i \quad (40)$$

For isothermal diffusion, the fluxes are related to the driving forces such as the gradient of the chemical potential by the generalized Maxwell-Stefan

equations (Krishna and Wesselingh, 1997)

$$\begin{aligned}\underline{d}_i &\equiv -\frac{x_i}{RT}\nabla_{T,p}\mu_i - \frac{1}{cRT}(c_i\bar{V}_i - \omega_i)\nabla p + \frac{1}{cRT}\left(c_i\underline{F}_i - \omega_i\sum_{k=1}^n c_k\underline{F}_k\right) \\ &= \sum_{j=1,i}^n \frac{x_j\underline{N}_i - x_i\underline{N}_j}{c\bar{D}_{ij}}, \quad i = 1, 2, \dots, n.\end{aligned}\quad (41)$$

where \underline{d}_i is the driving force acting on i per unit volume of the mixture, \underline{F}_i is the body force acting per unit mass of i , \underline{N}_i is the molar flux of i , x_i is the mole fraction, $c_i\bar{V}_i$ is the volume fraction of species i , ω_i is the mass fraction of i , and μ_i is the chemical potential of i and $\nabla_{T,p}\mu_i$ is the gradient of the chemical potential at a constant temperature T and pressure p . Here c , R , and \bar{D}_{ij} are the total concentration, the gas constant, and the Maxwell-Stefan diffusivity, respectively and n is the total number of species. As discussed in Bird et al. (2002, pp. 765-768), the first of (41) arises naturally in the expression for the entropy production rate $\dot{\sigma}$ in a multicomponent fluid mixture. The term \underline{d}_i is called a “driving force”, even though it does not have the dimensions of a force. However, $cRT\underline{d}_i$ may be regarded as a force per unit volume. The expression for $T\dot{\sigma}$ contains terms of the form $\sum_{i=1}^N \underline{j}_i \frac{cRT}{\rho_i} \underline{d}_i$, where \underline{j}_i is the mass flux of i relative to the mass average velocity and ρ_i is the density of i . Assuming that each flux j_i is a linear function of all the driving forces $\{\underline{d}_k\}$, the flux relations can be inverted to obtain the second of (41) (Curtiss and Bird, 1999). Predictions of (41) coupled with the mass balances agree fairly well with data obtained from many systems (Krishna and Wesselingh, 1997).

For isobaric diffusion in a dilute electrolyte solution, (41) can be simplified to obtain (Krishna, 1987)

$$\underline{N}_i = -D_i \nabla c_i - \frac{z_i c_i D_i F \nabla \phi_e}{RT} + c_i \underline{v} \quad (42)$$

where \underline{v} is the velocity vector of the solution, F is the Faraday constant, and ϕ_e is the electrostatic potential generated because of the ions. For a dilute system, the diffusivity \bar{D}_{ij} in (41) may be replaced by \bar{D}_{iw} i.e. the diffusivity of species i with respect to water. This quantity is defined as D_i in (42). Equation (42) is called the Nernst-Planck equation and has been used by many authors to model ion-exchange onto resins (Frey, 1986; Jia and Foutch, 2004; Bachet et al., 2014). In the context of defluoridation

with an oxide adsorbent, this approach has not been used earlier. During adsorption, it is assumed that the adsorbent and solution are electrically neutral separately.

The current density is given by

$$\underline{I} = \sum_{i=1}^n z_i \underline{N}_i F \quad (43)$$

or, using (42),

$$\underline{I} = \sum_{i=1}^n \left(z_i c_i \underline{v} - \frac{z_i^2 F^2 c_i D_i \nabla \phi_e}{RT} - z_i F D_i \nabla c_i \right) \quad (44)$$

As the system is electrically neutral, (31) and (44) imply that

$$\underline{I} = - \sum_{i=1}^n \left(\frac{z_i^2 F^2 c_i D_i \nabla \phi_e}{RT} + z_i F D_i \nabla c_i \right) \quad (45)$$

As no current passes through the system $I = 0$. Hence (45) reduces to

$$\nabla \phi_e = - \frac{RT \sum_{i=1}^n z_i D_i \nabla c_i}{F \sum_{i=1}^n z_i^2 c_i D_i} \quad (46)$$

Using standard electrochemical engineering terminology (Gu et al., 1997; Newman and Thomas-Alyea, 2012), the conductivity number κ and transport numbers t_i are defined by

$$\kappa \equiv \frac{F^2}{RT} \sum z_i^2 c_i D_i \quad (47)$$

$$t_i \equiv \frac{z_i^2 c_i D_i}{\sum_{k=1}^n z_k^2 c_k D_k} \quad (48)$$

Hence

$$\nabla \phi_e = - \frac{RT}{F} \frac{\sum_{i=1}^n z_i D_i \nabla c_i}{\kappa RT / F^2} \quad \text{and} \quad \frac{t_i}{z_i} = \frac{z_i c_i D_i}{\kappa RT / F^2} \quad (49)$$

Substituting (46) and (49) in (42), we obtain

$$\underline{N}_i = -D_i \nabla c_i + \frac{t_i}{z_i} \left[\sum_{k=1}^n z_k D_k \nabla c_k \right] + c_i \underline{v}$$

or

$$\underline{N}_i = - \sum_{j=1}^n \mathfrak{D}_{ij} \nabla c_j + c_i \underline{v} \quad (50)$$

where

$$\mathfrak{D}_{ij} \equiv \delta_{ij} D_i - \frac{t_i}{z_i} z_j D_j \quad (51)$$

and δ_{ij} is the Kronecker delta.

It may be noted that the fluxes are coupled to the driving forces of all the species due to enforcement of charge neutrality. Ignoring the axial diffusion and axial dispersion in the bulk liquid,

$$N_{i,z} = c_{i,b} v_z = \epsilon_b c_{i,b} \bar{v}_z \quad (52)$$

where $N_{i,z}$ is the z-component of the molar flux and \bar{v}_z is the interstitial velocity.

If we ignore convection in the liquid film, and if diffusion occurs only in the x-direction (Fig. 5), (50) reduces to

$$\tilde{N}_{i,x} = - \sum_{j=1}^n \mathfrak{D}_{ij} \frac{\partial c_j}{\partial x} \quad (53)$$

Ignoring the accumulation in the liquid film, and if the only reaction in the film is the dissociation of water, the mass balances are given by

$$\frac{d\tilde{N}_{i,x}}{dx} = 0; \quad i = 2, n-2 \quad (54)$$

$$\frac{d\tilde{N}_{i,x}}{dx} = \dot{R}_{i,f}; \quad i = 1 \text{ \& } i = n-1 \quad (55)$$

Following the procedure used earlier, equations (55) are combined to eliminate the rate of the decomposition of water and may be rewritten as

$$\frac{d\tilde{N}_{1,x}}{dx} - \frac{d\tilde{N}_{n-1,x}}{dx} = 0$$

The above equation can be integrated to obtain

$$\tilde{N}_{1,x} - \tilde{N}_{n-1,x} = \text{constant} \quad (56)$$

Assuming that the concentration varies linearly across the film, and using (53) in (56) we obtain

$$\tilde{N}_{1,x} - \tilde{N}_{n-1,x} = \sum_{j=1}^n (\mathfrak{D}_{1j} - \mathfrak{D}_{n-1,j}) \frac{(c_{j,b} - c_{j,s})}{\delta} \quad (57)$$

where $c_{j,b}$ is the concentration in the bulk liquid, $c_{j,s}$ is the concentration at the surface of the pellet, and δ is the thickness of the film (Fig. 5). Note that the \mathfrak{D}_{ij} 's are functions of the concentrations, but have been treated as constants while deriving (57) from (53). Similarly,

$$\tilde{N}_{i,x} = \sum_{j=1}^n \mathfrak{D}_{ij} \frac{(c_{j,b} - c_{j,s})}{\delta}; \quad i = 2, n-2 \quad (58)$$

The expressions derived for fluxes to the surface of the pellet can be substituted into the balances (38) and (39) for the bed. These reduce to

$$\frac{\partial}{\partial t} \left[\epsilon_b \left(c_{1,b} - \frac{K_w}{c_{1,b}} \right) \right] + \frac{\partial}{\partial z} \left[\epsilon_b \bar{v}_z \left(c_{1,b} - \frac{K_w}{c_{1,b}} \right) \right] = -a_p \sum_{j=1}^n (\mathfrak{D}_{1j} - \mathfrak{D}_{n-1,j}) \frac{(c_{j,b} - c_{j,s})}{\delta} \quad (59)$$

$$\frac{\partial}{\partial t} (\epsilon_b c_{i,b}) + \frac{\partial}{\partial z} (\epsilon_b \bar{v}_z c_{i,b}) = -a_p \sum_{j=1}^n \mathfrak{D}_{ij} \frac{(c_{j,b} - c_{j,s})}{\delta}; \quad i = 2, n-2 \quad (60)$$

Let us now consider the liquid inside the pellets. The mass balance are given by

$$\frac{\partial}{\partial t} (\epsilon_p c_{i,p}) + \nabla \cdot \underline{N}_{i,p} = \rho_p \dot{R}_{i,p} + \dot{R}_{i,x} \quad (61)$$

where ϵ_p is the porosity of the pellet, $c_{i,p}$ is the molar concentration of i per unit volume of the fluid, $\underline{N}_{i,p}$ is the molar flux of species i in the pellet, $\dot{R}_{i,p}$ is the molar rate of production of i per unit mass of the pellet, ρ_p is the density of the pellet, and $\dot{R}_{i,x}$ is the rate of production of i due to the water reaction (28). Thus

$$\dot{R}_{i,x} = 0; \quad i \neq 1 \text{ \& } i \neq n-1 \quad (62)$$

$$\dot{R}_{1,x} = \dot{R}_{n-1,x} \quad (63)$$

Subtracting the mass balance equation for $i = n-1$ from that of $i = 1$, we obtain

$$\frac{\partial}{\partial t} \left[\epsilon_p \left(c_{1,p} - \frac{K_w}{c_{1,p}} \right) \right] + \nabla \cdot [\underline{N}_{1,p} - \underline{N}_{n-1,p}] = \rho_p (\dot{R}_{1,p} - \dot{R}_{n-1,p}) \quad (64)$$

$$\frac{\partial}{\partial t} (\epsilon_p c_{i,p}) + \nabla \cdot \underline{N}_{i,p} = \rho_p \dot{R}_{i,p}; \quad i = 2, n-2 \quad (65)$$

To simplify the analysis, (64) and (65) are integrated over the the volume V_p of the pellet. Thus

$$\frac{\partial}{\partial t} \left[\epsilon_p V_p \left(\bar{c}_{1,p} - \frac{K_w}{\bar{c}_{1,p}} \right) \right] + \underline{n} \cdot [A_p (\underline{N}_{1,p} - \underline{N}_{n-1,p})]_{r=R_p} = \rho_p V_p (\bar{\dot{R}}_{1,p} - \bar{\dot{R}}_{n-1,p}) \quad (66)$$

$$\frac{\partial}{\partial t} (\epsilon_p V_p \bar{c}_{i,p}) + \underline{n} \cdot A_p \underline{N}_{i,p} \big|_{r=R_p} = \rho_p V_p \bar{\dot{R}}_{i,p}; \quad i = 2, n-2 \quad (67)$$

where overbars denote volume-averaged values, A_p is the external surface area of the pellet, \underline{n} is the unit outward normal, and R_p is the radius of the pellet (Fig. 5).

The pellets that are normally used for adsorption are porous materials, and hence the diffusion process may occur by bulk, Knudsen, and surface diffusion (Ruthven, 1984). Therefore, inside the pellets there will be an effective diffusion. Ignoring convection within the pellets, the flux of a species i in dilute electrolyte solution is given by an equation analogous to (50), i.e.

$$\underline{N}_{i,p} = - \sum_{j=1}^n \mathfrak{D}_{ij}^e \nabla c_{j,p} \quad (68)$$

where \mathfrak{D}_{ij}^e denotes an effective diffusion coefficient. The above equation is similar to the dusty gas model for a dilute mixture (Krishna and Wesselingh, 1997), but with the incorporation of an electrical force. Therefore

$$\mathfrak{D}_{ij}^e \equiv D_i^e \delta_{ij} - \frac{t_i}{z_i} z_j D_j^e \quad (69)$$

$$\frac{1}{D_i^e} = \frac{1}{D_{iw}^e} + \frac{1}{D_{im}^e}; \quad t_i = \frac{z_i^2 D_i^e c_{i,p}}{\sum_{j=1}^n z_j^2 D_j^e c_{j,p}} \quad (70)$$

where D_{iw}^e is an effective ion-water bulk diffusion coefficient, and D_{im}^e is an effective Knudsen diffusion coefficient of species i in the porous medium. In the present model, the Knudsen diffusion is neglected. For the porous medium, $D_i^e = D_{iw}^e = \epsilon_p^{3/2} D_i$ (Tjaden et al., 2016). The radial component of the flux is given by

$$\underline{n} \cdot \underline{N}_{i,p} = N_{i,p} \big|_r = - \sum_{j=1}^n \mathfrak{D}_{ij}^e \frac{\partial c_{j,p}}{\partial r} \quad (71)$$

In the spirit of the linear driving force model (Gleuckauf, 1955; Sircar and Hufton, 2000; Moreira et al., 2006; Tefera et al., 2014), we approximate $\left. \frac{\partial c_{j,p}}{\partial r} \right|_{r=R_p}$ by

$$\left. \frac{\partial c_{j,p}}{\partial r} \right|_{r=R_p} = \frac{c_{j,p,s} - \bar{c}_{j,p}}{\delta'} = \frac{c_{j,s} - \bar{c}_{j,p}}{\delta'} \quad (72)$$

where $\bar{c}_{j,p}$ is the volume averaged concentration of j in the pellet, $c_{j,p,s} = c_{j,s}$ is the value of c_j at the external surface of the pellet, and δ' is a constant. Hence the fluxes are given by

$$N_{1,p}|_{r=R_p} - N_{n-1,p}|_{r=R_p} = - \sum_{j=1}^n (\mathfrak{D}_{1j}^e - \mathfrak{D}_{n-1,j}^e) \frac{(c_{j,s} - \bar{c}_{j,p})}{\delta'} \quad (73)$$

$$N_{i,p}|_{r=R_p} = - \sum_{j=1}^n \mathfrak{D}_{ij}^e \frac{(c_{j,s} - \bar{c}_{j,p})}{\delta'}; \quad i = 2, n-2 \quad (74)$$

Using (72) and (71), (66) and (67) can be rewritten as

$$\frac{\partial}{\partial t} \left[\epsilon_p V_p \left(\bar{c}_{1,p} - \frac{K_w}{\bar{c}_{1,p}} \right) \right] - A_p \sum_{j=1}^n (\mathfrak{D}_{1j}^e - \mathfrak{D}_{n-1,j}^e) \frac{(c_{j,s} - \bar{c}_{j,p})}{\delta'} = \rho_p V_p (\bar{R}_{1,p} - \bar{R}_{n-1,p}) \quad (75)$$

$$\frac{\partial}{\partial t} (\epsilon_p V_p \bar{c}_{i,p}) - A_p \sum_{j=1}^n \mathfrak{D}_{ij}^e \frac{(c_{j,s} - \bar{c}_{j,p})}{\delta'} = \rho_p V_p \bar{R}_{i,p}; \quad i = 2, n-2 \quad (76)$$

The concentration $c_{j,s}$ in the above equations may be eliminated by ensuring the continuity of fluxes at the surface of the pellet. Thus

$$\tilde{N}_{1,x} - \tilde{N}_{n-1,x} = - (N_{1,p} - N_{n-1,p})|_{r=R_p} \quad (77)$$

$$\tilde{N}_{i,x} = - N_{i,p}|_{r=R_p}; \quad i = 2, n-2 \quad (78)$$

Substituting the fluxes we obtain

$$\sum_{j=1}^n (\mathfrak{D}_{1j} - \mathfrak{D}_{n-1,j}) \frac{(c_{j,b} - c_{j,s})}{\delta} = \sum_{j=1}^n (\mathfrak{D}_{1j}^e - \mathfrak{D}_{n-1,j}^e) \frac{(c_{j,s} - \bar{c}_{j,p})}{\delta'} \quad (79)$$

$$\sum_{j=1}^n \mathfrak{D}_{ij} \frac{(c_{j,b} - c_{j,s})}{\delta} = \sum_{j=1}^n \mathfrak{D}_{ij}^e \frac{(c_{j,s} - \bar{c}_{j,p})}{\delta'}; \quad i = 2, n-2 \quad (80)$$

Equations (79) and (80) involve n unknowns $c_{j,s}, j = 1, n$. However, as discussed earlier, the final form of the expressions for the fluxes in the bulk and

the pellet can be obtained by eliminating the species $n-1$ and n , and can be written as (see Appendix A)

$$\begin{aligned}\tilde{N}_{1,x} - \tilde{N}_{n-1,x} &= \sum_{j=1}^{n-2} k_{b,1j}(c_{j,b} - c_{j,s}), \\ \tilde{N}_{i,x} &= \sum_{j=1}^{n-2} k_{b,ij}(c_{j,b} - c_{j,s}); \quad i = 2, n-2\end{aligned}\tag{81}$$

$$\begin{aligned}(N_{1,p} - N_{n-1,p})|_{r=R_p} &= - \sum_{j=1}^{n-2} k_{p,1j}(c_{j,s} - \bar{c}_{j,p}), \\ N_{i,p}|_{r=R_p} &= - \sum_{j=1}^{n-2} k_{p,ij}(c_{j,s} - \bar{c}_{j,p}); \quad i = 2, n-2\end{aligned}\tag{82}$$

where $k_{b,ij}$ and $k_{p,ij}$ are effective mass transfer coefficients for transfer from the bulk solution to the surface of the pellet, and from the surface of the pellet to the interior, respectively. They are given by

$$\begin{aligned}k_{b,ij} &= \begin{cases} \lambda_{i1} - \frac{\phi}{c_{1,s}} \lambda_{i,n-1} & j = 1 \\ \lambda_{ij} & j \neq 1 \end{cases} \\ k_{p,ij} &= \begin{cases} \lambda'_{i1} - \frac{\phi'}{c_{1,s}} \lambda'_{i,n-1} & j = 1 \\ \lambda'_{ij} & j \neq 1 \end{cases} \end{aligned} \quad i = 1, n-2; j = 1, n-2 \tag{83}$$

where

$$\begin{aligned}\lambda_{ij} &= \begin{cases} \mathbb{D}_{ij} & i \neq 1 \\ \mathbb{D}_{1j} - \mathbb{D}_{n-1,j} & i = 1 \end{cases} \\ \lambda'_{ij} &= \begin{cases} \mathbb{D}'_{ij} & i \neq 1 \\ \mathbb{D}'_{1j} - \mathbb{D}'_{n-1,j} & i = 1 \end{cases} \end{aligned} \quad i = 1, n-2; j = 1, n-1 \tag{84}$$

$$\begin{aligned}\mathbb{D}_{ij} &= \frac{(\mathfrak{D}_{ij} - \xi_{jn} \mathfrak{D}_{in})}{\delta} \\ \mathbb{D}'_{ij} &= \frac{(\mathfrak{D}_{ij}^e - \xi_{jn} \mathfrak{D}_{in}^e)}{\delta'} \end{aligned} \quad i = 1, n-1; j = 1, n-1 \tag{85}$$

A detailed derivation is given in Appendix A. The quantities \mathfrak{D}_{ij} , \mathfrak{D}_{ij}^e are defined in (51) and (69), respectively, and ϕ , ϕ' , and ξ_{ij} in (83) - (85) are

defined by

$$\phi = \frac{K_w}{c_{1,b}}, \quad \phi' = \frac{K_w}{\bar{c}_{1,p}}, \quad \xi_{ij} = \frac{z_i}{z_j}$$

Equations (77) - (82) imply that

$$\sum_{j=1}^{n-2} k_{b,ij}(c_{j,b} - c_{j,s}) = \sum_{j=1}^{n-2} k_{p,ij}(c_{j,s} - \bar{c}_{j,p}); \quad i = 1, n-2 \quad (86)$$

Let us relate the balances in the stirred vessel to the balances in the bed. Integrating (59) over the volume of the bed and using (81), we obtain

$$\begin{aligned} V_b \frac{d}{dt} \left[\epsilon_b \left(\bar{c}_{1,b} - \frac{K_w}{\bar{c}_{1,b}} \right) \right] + A \epsilon_b \bar{v}_z \left[\left(c_{1,b} - \frac{K_w}{c_{1,b}} \right)_{z=L} - \left(c_{1,b} - \frac{K_w}{c_{1,b}} \right)_{z=0} \right] \\ = -a_p A \sum_{j=1}^{n-2} \int_0^L k_{b,1j}(c_{j,b} - c_{j,s}) dz \end{aligned} \quad (87)$$

where A is the area of cross section of the bed, and $\bar{c}_{1,b}$ is the volume averaged bulk concentration. As the solution is recirculated at a volumetric flow rate \dot{Q} , we have $\dot{Q} = A \epsilon_b \bar{v}_z$, $c_{1,b}|_{z=L} = c_{1,f}$, and $c_{1,b}|_{z=0} = c_1$ (see Fig. 4). Equation (87) can be rewritten as

$$\begin{aligned} \dot{Q} \left[\left(c_{1,f} - \frac{K_w}{c_{1,f}} \right) - \left(c_1 - \frac{K_w}{c_1} \right) \right] = -V_b \frac{d}{dt} \left[\epsilon_b \left(\bar{c}_{1,b} - \frac{K_w}{\bar{c}_{1,b}} \right) \right] \\ - a_p A \sum_{j=1}^{n-2} \int_0^L k_{b,1j}(c_{j,b} - c_{j,s}) dz \end{aligned} \quad (88)$$

Similarly, the balances (60) for $i = 2, n-2$ in the bulk liquid may be integrated over the volume of the bed to obtain

$$\dot{Q}(c_{i,f} - c_i) = -V_b \frac{d}{dt}(\epsilon_b \bar{c}_{i,b}) - a_p A \sum_{j=1}^{n-2} \int_0^L k_{b,ij}(c_{j,b} - c_{j,s}) dz; \quad i = 2, n-2 \quad (89)$$

Using (88) and (89), the mass balances (33) and (34) for the stirred vessel take the form

$$V \left(\frac{dc_1}{dt} - \frac{dc_{n-1}}{dt} \right) = -V_b \frac{d}{dt} \left[\epsilon_b \left(\bar{c}_{1,b} - \frac{K_w}{\bar{c}_{1,b}} \right) \right] - a_p A \sum_{j=1}^{n-2} \int_0^L k_{b,1j}(c_{j,b} - c_{j,s}) dz \quad (90)$$

$$V \frac{dc_i}{dt} = -V_b \frac{d}{dt}(\epsilon_b \bar{c}_{i,b}) - a_p A \sum_{j=1}^{n-2} \int_0^L k_{b,ij}(c_{j,b} - c_{j,s}) dz; \quad i = 2, n-2 \quad (91)$$

Using (73) - (76) and (82), we obtain

$$\sum_{j=1}^{n-2} k_{p,1j}(c_{j,s} - \bar{c}_{j,p}) = \frac{V_p}{A_p} \frac{\partial}{\partial t} \left[\epsilon_p \left(\bar{c}_{1,p} - \frac{K_w}{\bar{c}_{1,p}} \right) \right] - \frac{\rho_p V_p}{A_p} (\bar{R}_{1,p} - \bar{R}_{n-1,p}); \quad (92)$$

$$\sum_{j=1}^{n-2} k_{p,ij}(c_{j,s} - \bar{c}_{j,p}) = \frac{V_p}{A_p} \frac{\partial}{\partial t} (\epsilon_p \bar{c}_{i,p}) - \frac{\rho_p V_p}{A_p} \bar{R}_{i,p}; \quad i = 2, n-2 \quad (93)$$

Substituting (92) and (93) in (90) and (91), respectively, and using (86) the final form of the overall mass balance is given by

$$V \frac{dc'_i}{dt} = -V_b \frac{d}{dt} (\epsilon_b \bar{c}'_{i,b}) - \frac{a_p AV_p}{A_p} \int_0^L \left[\frac{\partial}{\partial t} (\epsilon_p \bar{c}'_{i,p}) - \rho_p \bar{R}'_{i,p} \right] dz; \quad i = 1, n-2 \quad (94)$$

where $c'_1 = c_1 - K_w/c_1$, $\bar{R}'_{1,p} = \bar{R}_{1,p} - \bar{R}_{n-1,p}$ and $c'_i = c_i$, $\bar{R}'_{i,p} = \bar{R}_{i,p}$; $i = 2, n-2$, subscripts p and b represent concentrations in the solution in the particle and the bulk, respectively, and an overbar represent the average concentration. As the volume of the bed V_b is $\ll V$, the volume of the stirred vessel, (94) may be approximated by

$$V \frac{dc'_i}{dt} = -\frac{a_p AV_p}{A_p} \int_0^L \left[\frac{\partial}{\partial t} (\epsilon_p \bar{c}'_{i,p}) - \rho_p \bar{R}'_{i,p} \right] dz; \quad i = 1, n-2 \quad (95)$$

and the mass balance on the adsorbate is

$$\frac{\partial \bar{q}_j}{\partial t} = \bar{R}'_{j,p}; \quad j = 1, m \quad (96)$$

4. Results and discussion

4.1. Adsorption of single components

Activated alumina (AA) is an amphoteric oxide because of its ability to accept and donate protons. During this process, based on the affinity of the sites on the adsorbent towards the ions, they are adsorbed on the surface. Therefore, in order to know the affinity of different ions for the adsorbent, experiments were conducted with F^- , HCO_3^- , SO_4^{2-} , NO_3^- , and Cl^- . Fluoride, HCO_3^- , and SO_4^{2-} were adsorbed on AA with an increase in the pH of the solution for F^- and SO_4^{2-} , but a decrease in the pH for HCO_3^- . An equilibrium was attained in 15-20 h for F^- (Fig. 6), and 5 h for SO_4^{2-} (Fig. 7). The uptake of SO_4^{2-} was very low. With respect to NO_3^- , there was

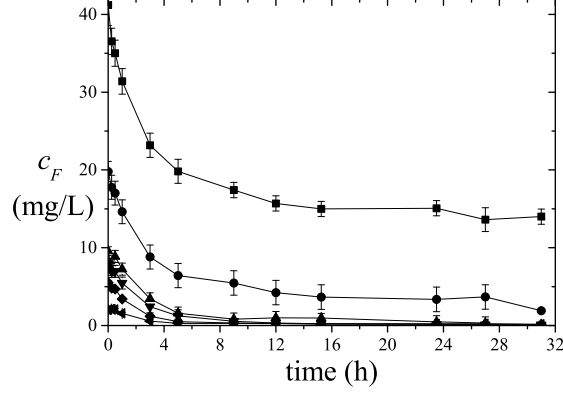


Figure 6: Variation of the concentration of F^- , c_F with time of operation for different initial concentrations of F^- in mg/L: \blacksquare , 40; \bullet , 20; \blacktriangle , 10; \blacktriangledown , 8; \blacklozenge , 5; \blacktriangleleft , 2. Mass of the adsorbent used $m_{AA} = 1.0$ g and volume of solution taken $V_s = 200$ mL.

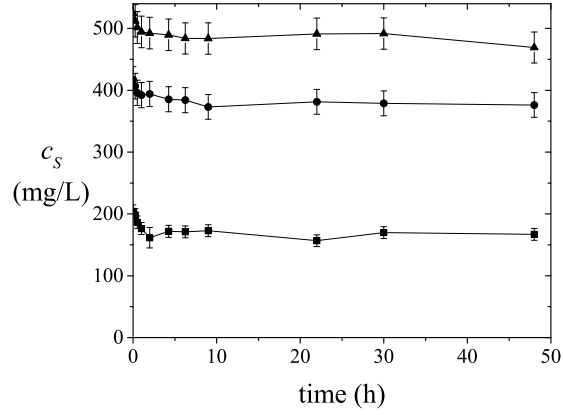


Figure 7: Variation of the concentration of SO_4^{2-} , c_S with the time of operation for different initial concentrations of SO_4^{2-} in mg/L : \blacktriangle , 524; \bullet , 417; \blacksquare , 204. Parameter values are as in Fig. 6.

a slight decrease in the concentration of NO_3^- in the solution at the start of the experiment, but after 1 h it was constant (Fig. 8). Therefore, there it can

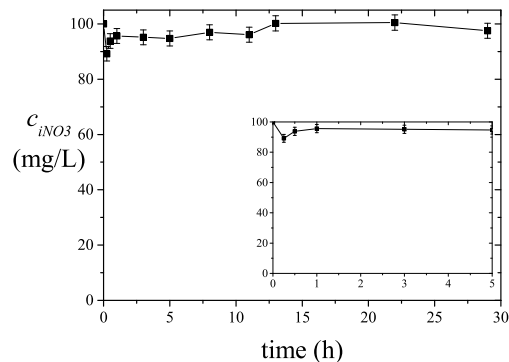


Figure 8: Variation of the concentration of NO_3^- , c_N with the time of operation for an initial concentration of 100 mg/L of NO_3^- . The inset shows the variation of c_N in the first few hours of operation. Parameter values are as in Fig. 6.

be assumed that there was no adsorption of NO_3^- onto AA. For Cl^- , there was a decrease in the concentration for 2-4 h, along with a leaching of NO_3^- into the solution (Fig. 9). This was probably because HNO_3 was used as a

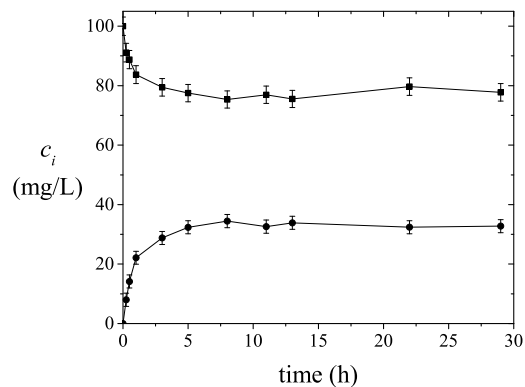


Figure 9: Variation of the concentration of species i , c_i with the time of operation for an initial concentration of 100 mg/L of Cl^- : \blacksquare , Cl^- ; \bullet , NO_3^- . Parameter values are as in Fig. 6.

binding agent during the manufacture of AA (Oxide India Pvt. Ltd., private

communication 2014). Even after soaking in DI water, some amount of NO_3^- might have remained on the adsorbent. Hence, the drop in Cl^- can be caused by an exchange of Cl^- and NO_3^- to maintain an electrically neutral solution. However, this argument does not hold during the adsorption of SO_4^{2-} and F^- . The leaching of NO_3^- has attained equilibrium after 1 h during the adsorption of SO_4^{2-} and after 4 h during the adsorption of F^- . Adsorption of HCO_3^- attained an equilibrium at about 10 h (Fig. 10) and there was a faster drop in the pH at lower concentrations of HCO_3^- compared to that with higher concentrations (Fig. 11).

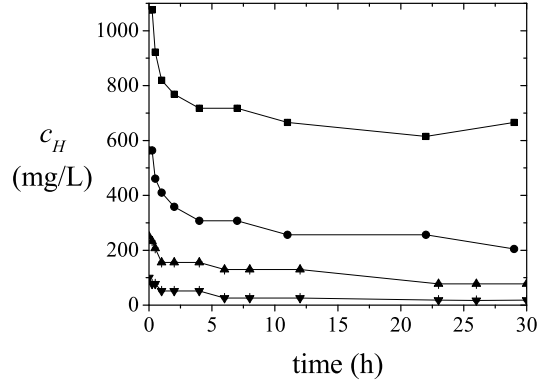
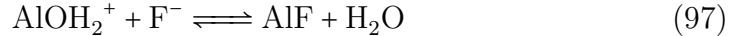


Figure 10: Variation of the concentration of HCO_3^- , c_H with the time of operation for different initial concentrations of HCO_3^- in mg/L: ■, 1076; ●, 563; ▲, 250; ▼, 100. Parameter values are as in Fig. 6.

In the case of ions which were adsorbed, there was either release or uptake of H^+ or OH^- , which causes a change in the pH. From some of the surface studies with the help of FTIR, it was predicted that the possible reactions of these ions with the adsorbent can be (Hao and Huang, 1986)



In the experiments with the shaker setup, discussed in section 2.1, there was no movement of the particles from the center of the flask. Therefore, to avoid this and get more reliable data, the differential bed adsorber setup was used for the experiments. It was observed that there was a considerable

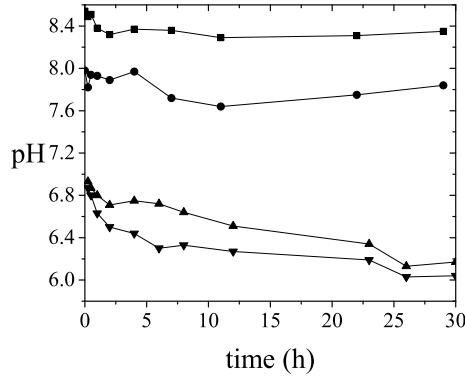


Figure 11: Variation of pH with the time of operation for different initial concentrations of HCO_3^- : ■, 1076; ●, 563; ▲, 250; ▼, 100. Parameter values are as in Fig. 6.

decrease in the external mass transfer resistance (Fig. 12). This can help in obtaining a better prediction of the kinetic results. However, no attempt was made to eliminate the mass transfer resistance completely in the experiments.

4.2. Negligible adsorption of NO_3^- , Cl^- , and Na^+ in the presence of F^-

For the selective removal of F^- from solutions, it is necessary to check for the dependence of the removal of F^- on the presence of other ions. These ions can either increase or decrease the uptake of F^- by the adsorbent. As the surface of AA is positively charged when the pH of the solution is below the pH of zero point charge (pH_{zpc}), it is possible for the surface to adsorb or attract anions. The converse is true if $\text{pH} > \text{pH}_{\text{zpc}}$. So the adsorption of F^- onto AA was checked in the presence of ions such as NO_3^- , Cl^- , and Na^+ .

There was no effect of Cl^- on the uptake of F^- (Fig. 13). This was reflected in the concentration of Cl^- , which shows that there was no adsorption of this ion onto the adsorbent (Fig. 14). However, when only Cl^- was present in the system, there was about 20% uptake (Fig. 9). This clearly indicates that the adsorption of Cl^- is mostly to neutralize the charge present on the surface of the adsorbent i.e. the ion that is present in the double layer (Fig. 2) rather than forming a new complex species on the adsorbent. As mentioned earlier, there was leaching of NO_3^- into the solution from the AA. When the concentrations of other ions such as F^- and Cl^- were increased, the leaching of NO_3^- into the solution was hindered, even though the value attained at

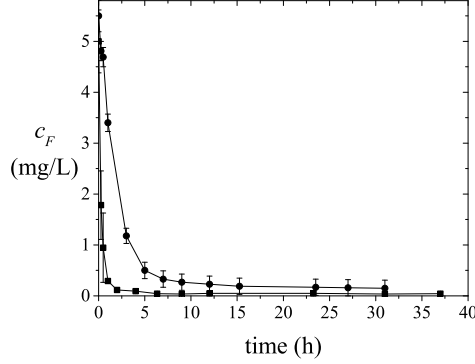


Figure 12: Variation of the concentration of F^- , c_F with the time of operation for an initial concentration of 5 mg/L of F^- : ■, differential bed adsorber; ●, shaker. The bulk density in both the experiments was kept at a constant value of 5 g/L. Volumetric flow rate for the differential bed adsorber = 1.5 mL/s.

long times was almost the same (Fig. 15). This delay may be caused by a decrease in the effective diffusion coefficient of NO_3^- , which is affected because of the higher concentration of Cl^- . Therefore, there is a relatively higher influx of Cl^- compared to the outflow of NO_3^- from the pellet.

Similarly, NO_3^- had a negligible effect on the adsorption of F^- (Fig. 16). For an initial NO_3^- concentration of 200 mg/L, there was an increase in the NO_3^- concentration because of the release of the nitrate from the adsorbent. For a higher initial concentration, there was no leaching (Fig. 17). This may be caused by a lower concentration gradient between the NO_3^- in the pellets and in the solution, which is responsible for the diffusion of NO_3^- into the solution.

The adsorption of positive ions onto AA is mainly assumed to occur when the surface is negatively charged, i.e. when the pH of the solution is $> pH_{zpc}$. In the presence of F^- , there was an increase in the pH of the solution upon adsorption of F^- (Fig. 18), but not $> pH_{zpc}$ of the adsorbent i.e. 7.8. The pH_{zpc} was obtained from the equilibrium constants K_1 and K_2 for the alumina using the equation (Charmas et al., 1995)

$$pH_{zpc} = \frac{1}{2}(pK_1 + pK_2) \quad (99)$$

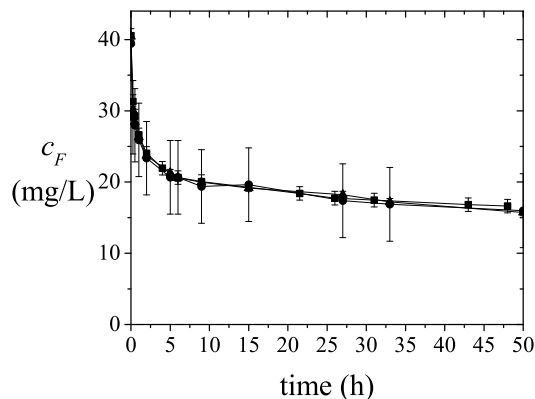


Figure 13: Variation of the concentration of F^- , c_F with the time of operation for an initial concentration of 40 mg/L of F^- and different initial concentrations of Cl^- in mg/L: ●, 800; ■, 200; ▲, 0. The bulk density was 5 g/L and the volumetric flow rate was 1.5 mL/s.

The values of K_1 and K_2 are determined in the next section. Therefore there were not many negative sites on the adsorbent for the adsorption or attraction of the Na^+ ions. This was observed in the negligible adsorption of Na^+ on AA (Fig. 19). In these experiments, the Na^+ ion was added in the form of NaF. Hence there was a simultaneous increase in concentration of both these ions. An increment of Na^+ with F^- maintained constant is possible by the addition of NaOH. However, this leads to an increase in the pH of the solution, thereby changing the initial condition for the adsorption of F^- . With NaF, there is negligible or no change in the pH of the solution.

4.3. Effect of soaking on the surface of the adsorbent

Soaking of activated alumina is observed to have profound effect on the surface and reactivity of the adsorbent. Kanwar (2010) observed that soaking of AA in deionized water for 24 h had increased the uptake of F^- compared to fresh AA or AA soaked for 48 h. Scanning electron microscope (SEM) images show that the fresh AA had a rough surface with many small particles on it (Fig. 20) but when the AA was soaked for 24 h, the surface was covered with hexagonal rings (Fig. 21). This indicates that there is some change in the crystalline structure of alumina and it might be the reason for an increased uptake of F^- . Upon adsorption of F^- , there is a change in structure to a

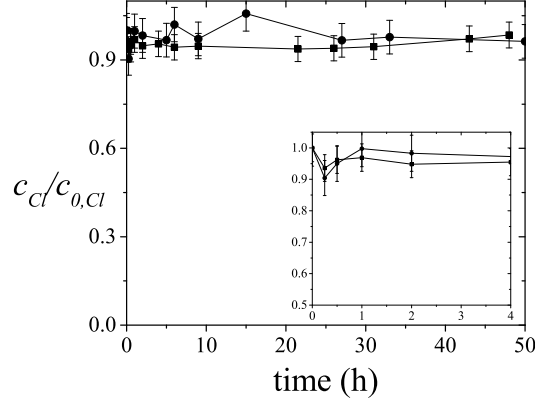


Figure 14: Variation of the concentration of Cl^- , c_{Cl} with the time of operation for an initial concentration of 40 mg/L of F^- and different initial concentrations of Cl^- ($c_{0,\text{Cl}}$) in mg/L: ●, 800; ■, 200. Parameter values are as in Fig. 13.

smooth surface with mostly large particles compared to fresh AA (Fig. 22).

4.4. Prediction of the concentrations of different ions

4.4.1. Estimation of the equilibrium constants

First consider the equilibrium titration data, obtained as discussed in section 2.3. To predict the variation of the pH with the volume of acid added, estimates for the equilibrium constants K_i , and the total number of sites on the adsorbent c_T are needed. As mentioned earlier, NO_3^- leaches from AA. In order to account for NO_3^- in (19), along with K_1, K_2 , and c_T , the initial concentration of nitrate present when the adsorbent is added to solution i.e. c_{imp} was also taken as a parameter.

Initial guesses for K_1, K_2 , and c_T were obtained from the results of Kanwar (2010), and an estimate for c_{imp} was obtained from the experiment conducted by soaking the adsorbent in DI water before the start of the experiment. The final values of the parameters were obtained using the MATLAB routine Lsqcurvefit. However, there was a large variation in the values of K_1 and K_2 for different initial guesses (Table 2). As the values of c_T and c_{imp} were approximately constant for different initial guesses, average values were used for these parameters.

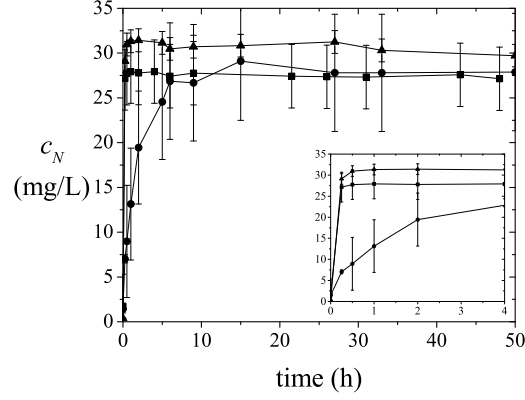


Figure 15: Variation of the concentration of NO_3^- , c_N with the time for an initial concentration of 40 mg/L of F^- and different initial concentrations of Cl^- in mg/L: \bullet , 800; \blacksquare , 200; \blacktriangle , 0. Parameter values are as in Fig. 13.

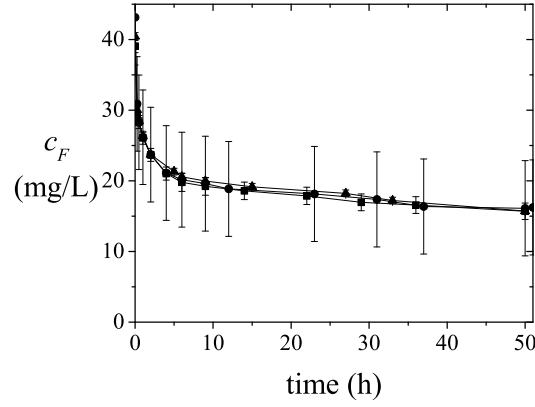


Figure 16: Variation of the concentration of F^- , c_F with the time for an initial concentration of 40 mg/L of F^- and different initial concentrations of NO_3^- in mg/L: \bullet , 800; \blacksquare , 200; \blacktriangle , 0. Parameter values are as in Fig. 13.

The constants are obtained by minimizing the objective function

$$f_o = \sum_i (F(p, xdata_i) - ydata_i)^2 \quad (100)$$

where $xdata_i$ and $ydata_i$ are the pH and the ratio of the volume of the acid

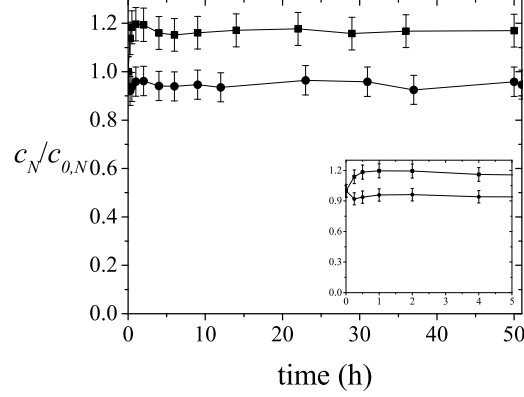


Figure 17: Variation of the concentration of NO_3^- , c_N with the time for an initial concentration of 40 mg/L of F^- and different initial concentrations of NO_3^- in mg/L: ●, 800; ■, 200. Parameter values are as in Fig. 13.

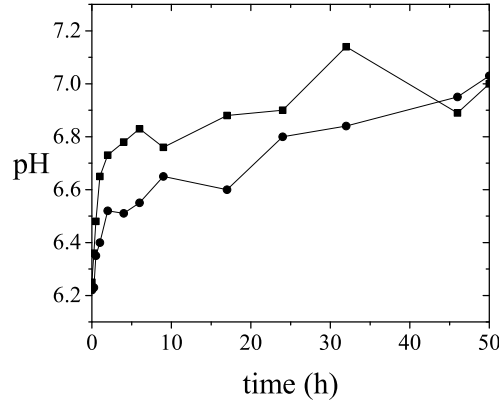


Figure 18: Variation of the pH with time for different concentrations of Na^+ and F^- in mg/L: ●, $c_{\text{Na}} = 14.6$ mg/L, $c_{\text{F}} = 9.2$ mg/L; ■, $c_{\text{Na}} = 22.6$ mg/L, $c_{\text{F}} = 14.4$ mg/L. Parameter values are as in Fig. 13.

added V_a to the volume of base taken V_b , respectively, corresponding to the i^{th} data point, and $F(p, xdata_i)$ is the predicted value of V_a/V_b , obtained using (19). Here p denotes the parameters that have to be estimated. Keeping c_T and c_{imp} fixed, contours of constant f_o are plotted in the pK_1 - pK_2 plane,

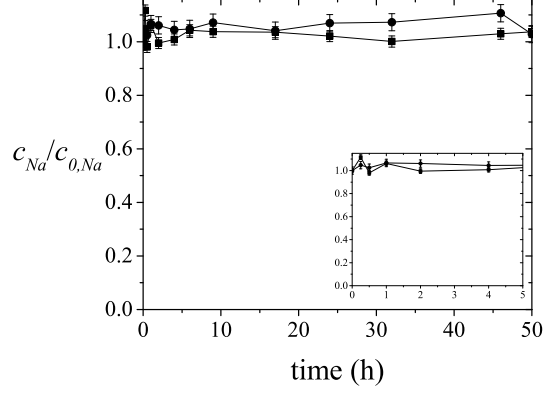


Figure 19: Variation of the dimensionless concentration of Na^+ , c_{Na} with time for different concentrations of Na^+ and F^- : \bullet , $c_{Na} = 14.6$ mg/L, $c_F = 9.2$ mg/L; \blacksquare , $c_{Na} = 22.6$ mg/L, $c_F = 14.4$ mg/L. Parameter values are as in Fig. 13.

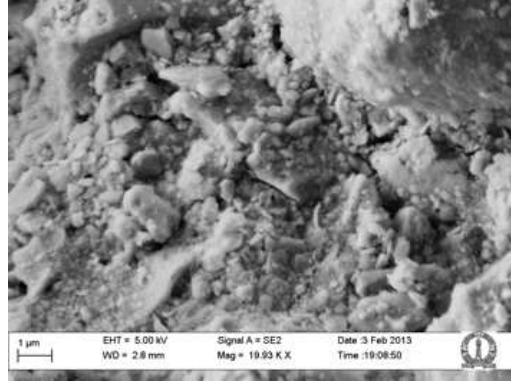


Figure 20: Scanning electron microscope image of fresh AA. Magnification ≈ 20 KX.

where $\text{p}K_i \equiv -\log_{10}K_i$. The minimum value of f_o occurs at $K_1 = 1.58 \times 10^6$ and $K_2 = 3.98 \times 10^{-10}$. The poor performance of Lsqcurvefit may be because of a shallow region near the minimum (Fig. 23). A good fit was obtained with $f_o = 0.0036$ (Fig. 24). The amount of impurity in the adsorbent in the form of NO_3^- i.e. $c_{imp}/\rho_b = 3.8$ mmol/g is more than the total number of sites ($c_T = 0.28$ mmol/g) on the adsorbent (Table 2). Thus NO_3^- is probably not adsorbed, but remains in the liquid in the pores of the adsorbent. This is also consistent with our assumption that NO_3^- and Cl^- are the ions which are

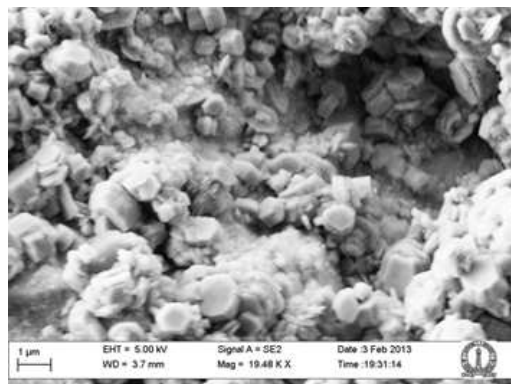


Figure 21: Scanning electron microscope image of AA soaked for 24 h. Magnification ≈ 20 KX.

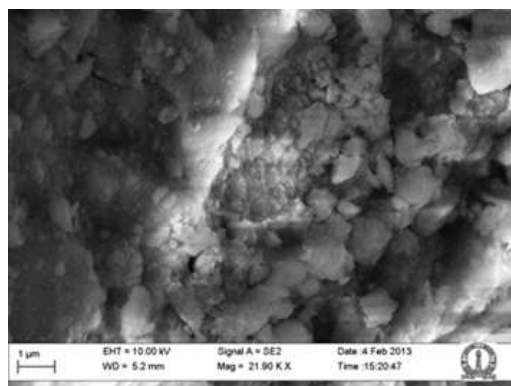


Figure 22: Scanning electron microscope image of AA after adsorption of F^- . Magnification ≈ 20 KX.

present only in the double layer adjacent to the charged surface as a means to counter the charge of the surface. The obtained pK values i.e. 6.2 and 9.4, correspond to the range of values reported in literature (Davis et al., 1978; Ryazanov and Dudkin, 2003, 2004). Sensitivity analysis for the obtained equilibrium constants K_1 and K_2 was done by varying the values by 20%. The simulated curves were similar to the values corresponding to the minimum f_o (Fig. 25).

In order to estimate the equilibrium constants for the adsorption of ions such as F^- and HCO_3^- , batch adsorption data and equilibrium values are

Table 2: Estimated parameters for the titration data using the MATLAB routine Lsqcurve-fit for three different initial guess values.

Parameter	initial guess			final value		
	1	2	3	1	2	3
$K_1 * 10^{-6}$	0.1	1.0	100	5.74	1.66	100
$K_2 * 10^9$	3.16	31.6	1.0	83.2	0.635	1.03
c_T (mmol/g)	0.115	0.12	0.042	0.236	0.277	0.24
c_{imp} (mol/L)	0.2	0.018	0.02	0.018	0.017	0.02

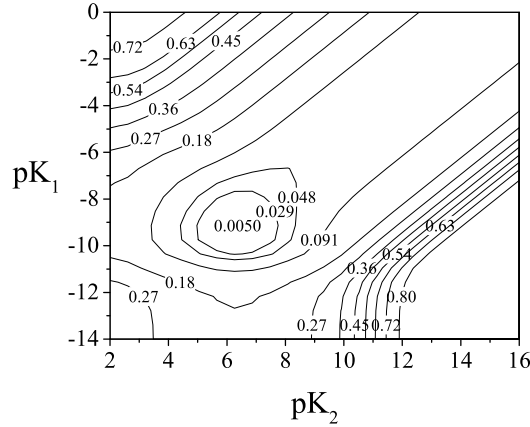


Figure 23: Contour map showing the variation of the objective function f_o with change in the values of $pK_1 = -\log_{10}K_1$ and $pK_2 = -\log_{10}K_2$.

required for a series of initial concentrations. Using the equilibrium data for F^- , Cl^- and H^+ (Fig. 26), the equilibrium constant K_3 (corresponding to (9)) was obtained by minimizing the objective function. During the adsorption experiment, it was observed that even after soaking AA in DI water there was still some amount of impurity present in the adsorbent. So, in order to

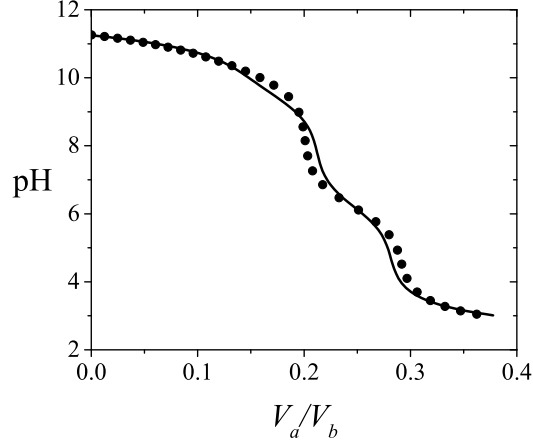


Figure 24: Titration of a solution containing 0.02 N NaOH and 0.25 g of AA with 0.02 N HCl: ●, data; —, model. Here $V_b = 50$ mL is the volume of the base taken and V_a is the volume of the acid added.

account for this a parameter q_{1i} (see (21)) is also taken into account along with K_3 . The objective function (100) was minimized using the MATLAB routine Lsqcurvefit and the parameters obtained were $K_3 = 1.66 \times 10^2$ and $q_{1i} = 0.13$ mmol/g. The model ((20) - (24)) fits the data for H^+ fairly well (Fig. 26), but overestimates the data for F^- and Cl^- at higher concentrations (Figs. 27 and 28).

4.4.2. Estimation of the rate constants for the reactions (7) - (9)

The rate expressions for these reactions (7) - (9) are given as

$$r_1 = k_{f1}(c_1q_2 - q_1/K_1) \quad (101)$$

$$r_2 = k_{f2}(q_2 - q_3c_1/K_1) \quad (102)$$

$$r_3 = k_{f3}(q_1c_2 - q_4/K_3) \quad (103)$$

where q_1 , q_2 , and q_3 correspond to the adsorbate concentrations of $\equiv AlOH_2^+Cl^-$, $\equiv AlOH$, and $\equiv AlO^-Na^+$, respectively. For the differential adsorber, the variation of the concentration of the ions with time can be obtained by integrating (95) and (96), and the mass balances for the adsorbates simultaneously. In order to solve these equations the values of the diffusivities D_i ,

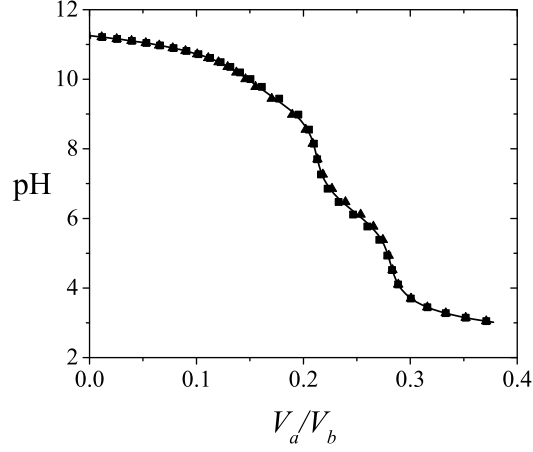


Figure 25: Simulated titration curves for titration of a solution containing 0.02 N NaOH and 0.25 g of AA with 0.02 N HCl: —●—, K_1 and K_2 corresponding to the minimum of f_o ($K_1 = 1.58 * 10^6 \equiv K_{1*}$, $K_2 = 3.98 * 10^{-10} \equiv K_{2*}$); —▲—, $K_2 = 0.8K_{2*}$, $K_1 = 0.8K_{1*}$; —■—, $K_2 = 1.2K_{2*}$, $K_1 = 1.2K_{1*}$. Here $V_b = 50$ mL is the volume of the base taken and V_a is the volume of the acid added.

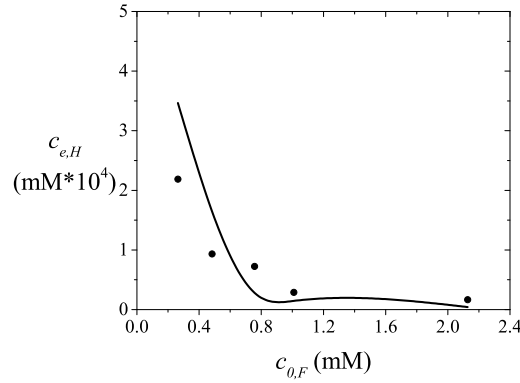


Figure 26: Variation of the equilibrium concentration of H^+ ($c_{e,H}$) with the initial concentration of F^- ($c_{0,F}$): —●—, data; —, model predictions.

the film thickness in bulk phase δ and in the pellet phase δ' , the rate constants for the reactions k_{fi} , and the surface concentrations $c_{j,s}$ are required.

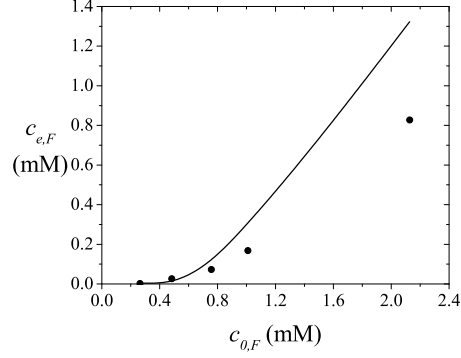


Figure 27: Variation of the equilibrium concentration of F^- ($c_{e,F}$) with the initial concentration of F^- ($c_{0,F}$): ●, data; —, model predictions.

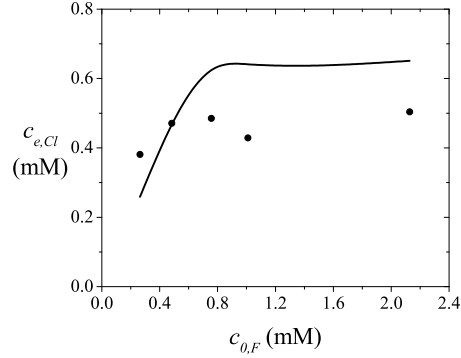


Figure 28: Variation of the equilibrium concentration of $\text{Cl}^- + \text{NO}_3^-$ ($c_{e,Cl}$) with the initial concentration of F^- ($c_{0,F}$): ●, data; —, model predictions.

The values of the diffusion coefficients were obtained from Cussler (2009) (Table 3). The film thickness in the bulk phase was obtained from the correlation (Wakao and Funazkri, 1978; Ruthven, 1984)

$$\delta = \frac{d_p}{2 + 1.1 \text{Sc}^{(1/3)} \text{Re}^{0.6}}, \quad 3 < \text{Re} < 10^4 \quad (104)$$

and in the pellet phase it was taken as $\delta' = d_p/10$ (Liaw et al., 1979; Seader and Henley, 2006). Using (79) and (80), the the surface concentrations can be calculated

Table 3: Diffusion coefficients at infinite dilution used for different ions.

Ion	D_{iw} (m ² /s)
H ⁺	$9.31 * 10^{-9}$
Na ⁺	$1.33 * 10^{-9}$
F ⁻	$1.47 * 10^{-9}$
Cl ⁻	$2.03 * 10^{-9}$
OH ⁻	$5.28 * 10^{-9}$

for known concentrations in the bulk and the particle phases. This was obtained using a modified Gauss elimination method, which is discussed in Appendix B.

As there are no predetermined values for the rate constants, an initial estimate was obtained for the special case of negligible diffusional resistance, and the rate constants were spanned over a range of values to obtain a minimum for the objective function. The minimum was obtained using an inhouse code . In the developed routine, the differential equations are solved using the MATLAB inbuilt routine ODE15s, which works well for a system of stiff equations. For an initial condition $c_{0,F} = 0.48$ mM and $c_{0,H} = 6.02 * 10^{-4}$ mM, the above equations were solved. Values of the objective function f_o , defined by an equation similar to (100), were plotted with respect to different values of the rate constants. Here, the $xdata_i$ and $ydata_i$ correspond to the dimensionless time and the experimental concentrations of all the ions at i , and $F(p, xdata_i)$ is the simulated dimensionless concentrations with parameters p . For each value of k_{f1} , contours of constant f_o in the $\log k_{f2}$ - $\log k_{f3}$ plane are shown in Fig. 29. It was found that there was a minimum value of f_o for each value of k_{f1} . This is denoted by $\min(f_o)$, and its variation with k_{f1} is shown in Fig. 30. The minimum value of f_o was obtained for the rate constants $k_{f1} = 1.59 * 10^4$ m³mol⁻¹s⁻¹, $k_{f2} = 1.0 * 10^{-9}$ s⁻¹, and $k_{f3} = 3.16 * 10^4$ m³mol⁻¹s⁻¹. Reasonably good fits were obtained for all the ions (Figs. 31 - 33).

The predicted rate constants were used to simulate the concentration profiles for initial F⁻ concentrations of 0.26 mM, 0.79 mM, and 1.05 mM, but the profiles did not fit the data well (Figs. 34 - 36). In Fig. 35, c_{Cl} increases with time because NO₃⁻ is released into the solution and Cl⁻ and

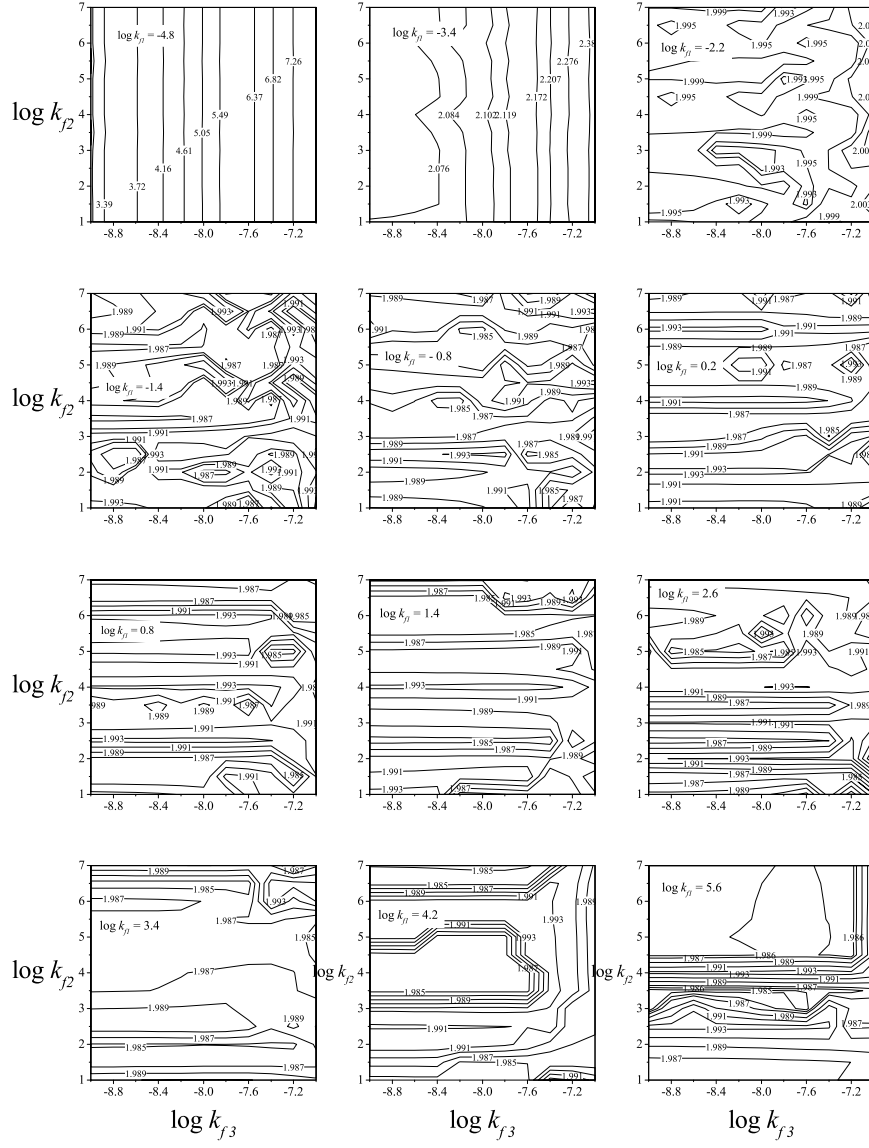


Figure 29: Contour map showing the variation of the objective function f_o with of k_{f1} , k_{f2} , and k_{f3} when diffusional resistance was considered. Each panel corresponds to a fixed value of k_{f1} .

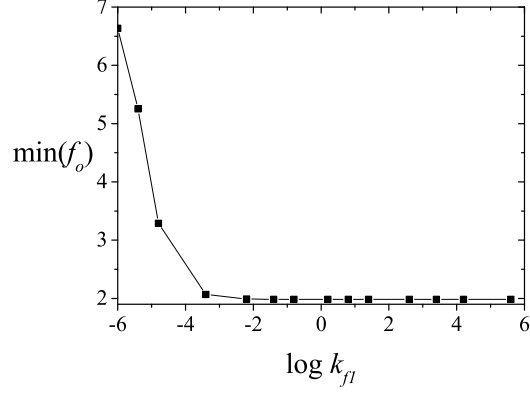


Figure 30: Variation with k_{f1} of the minimum value of the objective function $\min(f_o)$ obtained for different values of k_{f2} and k_{f3} .

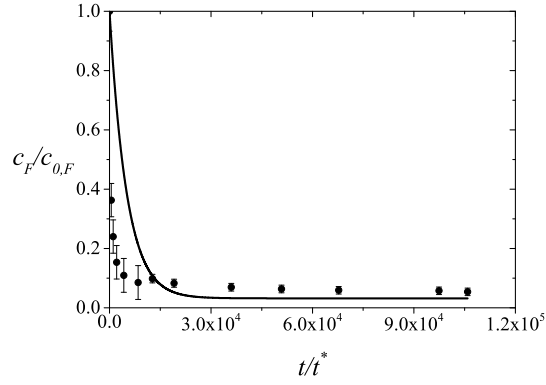


Figure 31: Variation of the dimensionless concentration of F^- ($c_F/c_{0,F}$) with dimensionless time of operation (t/t^*): \bullet , data; — , model predictions. Here $c_{0,F} = 0.48$ mM is the initial concentrations of F^- and $t^* = 1.7$ s is the empty bed contact time.

NO_3^- have been treated as interchangeable in the present work. There is an inherent error in the predictions at long times, as the theoretical equilibrium values for higher initial concentrations of F^- did not match the data (Figs. 26 - 28). The assumption of neutralizing the charge on the surface of pellet with a counter ion from the solution may be affecting the equilibrium and kinetics

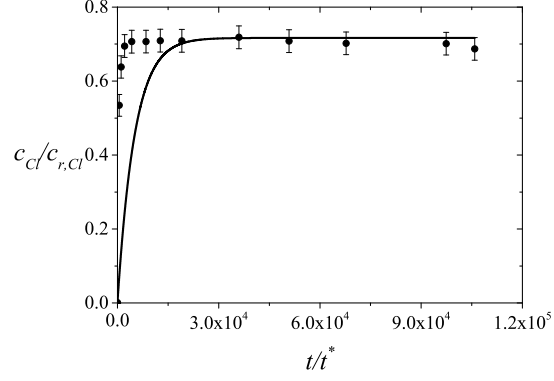


Figure 32: Variation of the dimensionless concentration of $\text{Cl}^- + \text{NO}_3^-$ ($c_{Cl}/c_{r,Cl}$) with dimensionless time of operation (t/t^*): \bullet , data; — , model predictions. Here $c_{0,F} = 0.48$ mM is the initial concentration of F^- , $c_{r,Cl} = \rho_b q_{1i} = 0.655$ mM is the maximum amount of impurity present on the adsorbent, and $t^* = 1.7$ s is the empty bed contact time.

of ion adsorption.

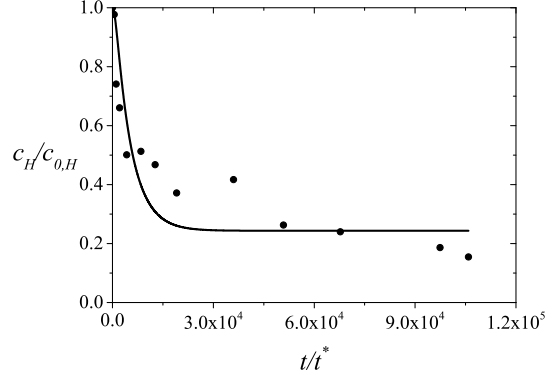


Figure 33: Variation of the dimensionless concentration of H^+ ($c_H/c_{0,H}$) with dimensionless time of operation (t/t^*): \bullet , data; — , model predictions. Here $c_{0,F} = 0.48$ mM, $c_{0,H} = 6.02 \times 10^{-4}$ mM are the initial concentration of F^- and H^+ , respectively, and $t^* = 1.7$ s is the empty bed contact time.

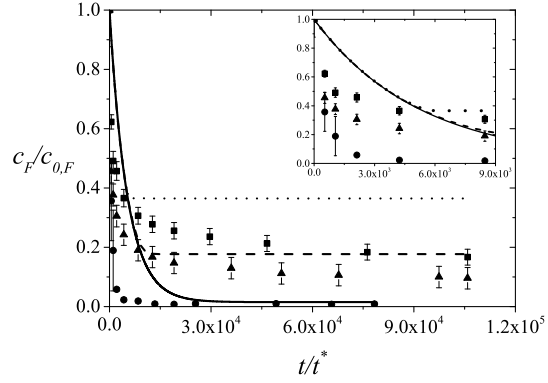


Figure 34: Variation of the dimensionless concentration of F^- ($c_F/c_{0,F}$) with dimensionless time of operation (t/t^*): \bullet , — , $c_{0,F} = 0.26$ mM; \blacktriangle , ----- , $c_{0,F} = 0.79$ mM; \blacksquare , , $c_{0,F} = 1.05$ mM; symbols, data; curves, predictions. Here $c_{0,F}$ is the initial concentration of F^- and $t^* = 1.7$ s is the empty bed contact time.

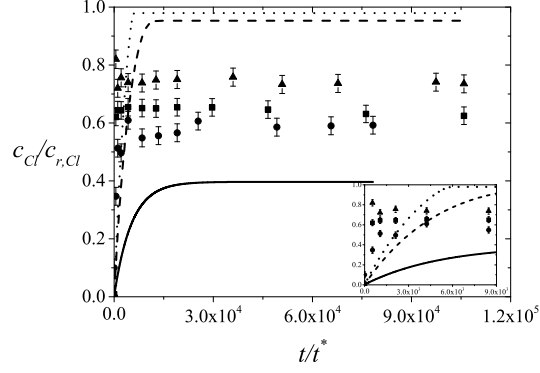


Figure 35: Variation of the dimensionless concentration of $\text{Cl}^- + \text{NO}_3^-$ ($c_{Cl}/c_{r,Cl}$) with dimensionless time of operation (t/t^*): \bullet , —, $c_{0,F} = 0.26$ mM; \blacktriangle , ----, $c_{0,F} = 0.79$ mM; \blacksquare , , $c_{0,F} = 1.05$ mM; symbols, data; curves, predictions. Here $c_{r,Cl} = \rho_b q_{1i} = 0.655$ mM and $t^* = 1.7$ s is the empty bed contact time.

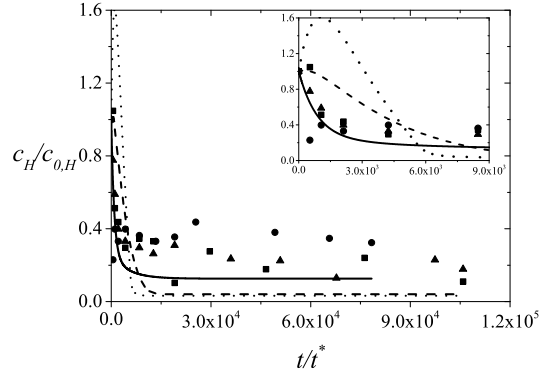


Figure 36: Variation of the dimensionless concentration of H^+ ($c_H/c_{0,H}$) with dimensionless time of operation (t/t^*): \bullet , —, $c_{0,F} = 0.26$ mM; \blacktriangle , ----, $c_{0,F} = 0.79$ mM; \blacksquare , , $c_{0,F} = 1.05$ mM; symbols, data; curves, predictions. Here $c_{0,H}$ is the initial concentration of H^+ and $t^* = 1.7$ s is the empty bed contact time.

5. Conclusions

The adsorption of F^- on activated alumina is observed to be highly influenced by the presence of many ions like HCO_3^- , SO_4^{2-} . Here single component adsorption of the ions was performed. There was adsorption of HCO_3^- and SO_4^{2-} , but a negligible adsorption of Cl^- , NO_3^- , and Na^+ onto AA. When a two-component adsorption was performed with F^- , there was no influence of Cl^- , NO_3^- , and Na^+ on the uptake of F^- .

Equilibrium constants for the reactions (7) and (8) were estimated by fitting model predictions to data obtained by titration. A good fit was obtained for the variation of the pH with the volume of acid added. The present model predicts the concentration profiles of the ions including H^+ , whereas existing models specify the concentration of H^+ and predict the equilibrium concentrations of the ion that is adsorbed. Here the formation of $\equiv AlF$ sites is dependent on all the sites and species in solution. For the reaction (9) i.e. the adsorption of F^- , a reasonable fit was obtained for the variation of equilibrium values of F^- , H^+ , and Cl^- with the initial concentration of F^- ($c_{0,F}$) in the range 0.3 - 0.8 mM. However, for $c_{0,F}$ in the range of 0.8 - 2.0 mM, the agreement between the model predictions and the data was not good.

A model describing the kinetics of adsorption in a differential bed adsorber was developed, accounting for the various ions in solution. For $c_{0,F} = 0.48$ mM, rate constants for the reactions (7) - (9) were estimated by fitting predictions to data. For other values of $c_{0,F}$, the performance of the model was not good.

Appendix A. Derivation of (81) and (82)

The derivation of (81) is discussed in this appendix. A similar approach can be used to derive (82). The flux terms used in the mass balance equations with the assumption of a linear driving force depend on the n species present in the system. But the dependence on the n species can be reduced to $n - 2$ species with the use of charge neutrality condition and the assumption that the water dissociation reaction attains equilibrium very rapidly. The general flux term is given by

$$N_i = \sum_{j=1}^n \mathfrak{D}_{ij} \frac{\Delta c_j}{\delta}, \quad i = 1, n \quad (A.1)$$

where $\mathfrak{D}_{ij} = D_i \delta_{ij} - \frac{t_i}{z_i} z_j D_j$, Δc_j is the difference in the concentration of species in the phases separated by a film of thickness δ . Let $i = 1$ denote H^+ , $i = n - 1$

denote OH^- , and $i = n$ be the species eliminated by the charge neutrality condition.

Using the assumption that the solution is electrically neutral, we have

$$\sum_{i=1}^n z_i c_i = 0 \quad (\text{A.2})$$

and substituting (A.2) in (A.1), we obtain

$$N_i = - \sum_{j=1}^{n-1} \xi_{nj} \mathfrak{D}_{in} \frac{\Delta c_j}{\delta} + \sum_{j=1}^{n-1} \mathfrak{D}_{ij} \frac{\Delta c_j}{\delta} \quad (\text{A.3})$$

where $\xi_{ij} = z_j/z_i$. If $\mathbb{D}_{ij} = \frac{\mathfrak{D}_{ij} - \xi_{ij} \mathfrak{D}_{in}}{\delta}$, then (A.3) can be rewritten as

$$N_i = \sum_{j=1}^{n-1} \mathbb{D}_{ij} \Delta c_j \quad (\text{A.4})$$

Now using the condition that the water reaction is very fast, we have

$$c_{n-1} = \frac{K_w}{c_1} \quad (\text{A.5})$$

Equations (A.4) and (A.5) imply that

$$N_i = \mathbb{D}_{i,n-1} K_w \left(\frac{1}{c_{1,b}} - \frac{1}{c_{1,s}} \right) + \sum_{j=1}^{n-2} \mathbb{D}_{ij} \Delta c_j \quad (\text{A.6})$$

$$N_i = \mathbb{D}_{i,n-1} K_w \frac{c_{1,s} - c_{1,b}}{c_{1,b} c_{1,s}} + \sum_{j=1}^{n-2} \mathbb{D}_{ij} \Delta c_j$$

Let $\phi = \frac{K_w}{c_{1,b}}$, then

$$\begin{aligned} N_i &= -\frac{\phi}{c_{1,s}} \mathbb{D}_{i,n-1} \Delta c_1 + \sum_{j=1}^{n-2} \mathbb{D}_{ij} \Delta c_j \\ N_i &= (\mathbb{D}_{i1} - \frac{\phi}{c_{1,s}} \mathbb{D}_{i,n-1}) \Delta c_1 + \sum_{j=2}^{n-2} \mathbb{D}_{ij} \Delta c_j, \quad i = 1, n \end{aligned} \quad (\text{A.7})$$

For $i = 2, n - 2$ and $i = n$, N_i can be written in the simplified form (81), with $\lambda_{ij} = \mathbb{D}_{ij}$. For $i = 1$ (57) implies that

$$\begin{aligned} N_1 - N_{n-1} &= (\mathbb{D}_{11} - \frac{\phi}{c_{1,s}} \mathbb{D}_{1,n-1}) \Delta c_1 + \sum_{j=2}^{n-2} \mathbb{D}_{1j} \Delta c_j \\ &\quad - (\mathbb{D}_{n-1,1} - \frac{\phi}{c_{1,s}} \mathbb{D}_{n-1,n-1}) \Delta c_1 - \sum_{j=2}^{n-2} \mathbb{D}_{n-1,j} \Delta c_j \end{aligned}$$

If $\lambda_{1j} = \mathbb{D}_{1j} - \mathbb{D}_{n-1,j}$, then

$$N_1 - N_{n-1} = -\frac{\phi}{c_{1,s}} \lambda_{1,n-1} \Delta c_1 + \sum_{j=1}^{n-2} \lambda_{1j} \Delta c_j \quad (\text{A.8})$$

Equation (A.8) can be written in terms of an effective mass transfer coefficient as

$$N_i = \sum_{j=1}^{n-2} k_{b,ij} \Delta c_j \quad (\text{A.9})$$

where $k_{b,ij}$ is given by (83). Using a similar approach, expressions for $k_{p,ij}$, which are shown in (83), can be derived.

Appendix B. Modified Gauss elimination to calculate the surface concentration

Calculation of the surface concentration is dependent on the concentrations of species in the bulk and the particle. As there is no accumulation of the mass in the films at the interfaces, there is a continuity in the flux from the bulk to particle. So, we obtain (79) and (80), and based on the derivation given in Appendix A, they can be modified as

$$\sum_{j=1}^{n-2} k_{b,ij} (c_{j,b} - c_{j,s}) = \sum_{j=1}^{n-2} k_{p,ij} (c_{j,s} - \bar{c}_{j,p}) \quad (\text{B.1})$$

Upon rearranging the terms we obtain

$$\sum_{j=1}^{n-2} c_{j,s} (k_{b,ij} + k_{p,ij}) = \sum_{j=1}^{n-2} (k_{b,ij} c_{j,b} + k_{p,ij} \bar{c}_{j,p}) \quad (\text{B.2})$$

Equation (B.2) can be represented in a matrix form by introducing effective mass transfer coefficients matrices $[k_b]$ and $[k_p]$ of size $[n - 2 \times n - 2]$ and concentration vectors c_s, c_p, c_b of size $n - 2$. The resulting matrix form will be

$$[k_b + k_p]c_s = [k_b]c_b + [k_p]c_p \quad (\text{B.3})$$

Equation (B.3) is of the form $AX = B$ and can be solved using Gauss elimination to obtain the unknown vector X if A and B are independent of the components of X . In the present case, the matrices are dependent on $c_{1,s}$. So, (B.3) is modified to solve for the vector c_s .

Using (83) for any i , from (B.3) we can obtain

$$\begin{aligned} -(\phi\lambda_{i,n-1} + \phi'\lambda'_{i,n-1}) + \sum_{j=1}^{n-2} (\lambda_{ij} + \lambda'_{ij})c_{j,s} = & -(\phi\lambda_{i,n-1}c_{1,b} + \phi'\lambda'_{i,n-1}\bar{c}_{1,p})\frac{1}{c_{1,s}} \\ & + \sum_{j=1}^{n-2} (\lambda_{ij}c_{j,b} + \lambda'_{ij}\bar{c}_{1,p}) \end{aligned} \quad (\text{B.4})$$

Upon rearranging and multiplying both sides by $c_{1,s}$ we obtain

$$\begin{aligned} (\lambda_{i1} + \lambda'_{i1})c_{1,s}^2 + \sum_{j=2}^{n-2} (\lambda_{ij} + \lambda'_{ij})c_{1,s}c_{j,s} + \left[-\sum_{j=1}^{n-2} (\lambda_{ij}c_{j,b} + \lambda'_{ij}\bar{c}_{j,p}) - \phi\lambda_{i,n-1} - \phi'\lambda'_{i,n-1} \right] c_{1,s} \\ + \phi\lambda_{i,n-1}c_{1,b} + \phi'\lambda'_{i,n-1}\bar{c}_{1,p} = 0 \end{aligned} \quad (\text{B.5})$$

If

$$\tau_{i,j-1} = \lambda_{ij} + \lambda'_{ij}; \quad j = 2, n-2; \quad i = 1, n-2 \& n \quad (\text{B.6})$$

$$\tau_{i,n-2} = \lambda_{i1} + \lambda'_{i1}; \quad i = 1, n-2 \& n \quad (\text{B.7})$$

$$\tau_{i,n-1} = -\sum_{j=1}^{n-2} (\lambda_{ij}c_{j,b} + \lambda'_{ij}\bar{c}_{j,p}) - \phi\lambda_{i,n-1} - \phi'\lambda'_{i,n-1}; \quad i = 1, n-2 \& n \quad (\text{B.8})$$

$$\tau_{v,i} = -(\phi\lambda_{i,n-1}c_{1,b} + \phi'\lambda'_{i,n-1}\bar{c}_{1,p}); \quad i = 1, n-2 \& n \quad (\text{B.9})$$

then (B.5) becomes

$$\sum_{j=2}^{n-2} (\tau_{i,j-1}c_{j,s}c_{1,s}) + \tau_{i,n-2}c_{1,s}^2 + \tau_{i,n-1}c_{1,s} = \tau_{v,i} \quad (\text{B.10})$$

Now $[\tau]$ is a matrix of dimension $[n - 2 \times n - 1]$ and τ_v is a vector of dimension $n - 2$. Using (B.10), a new unknown vector P can be defined with elements being $c_{j,s}c_{1,s}$ ($j = 2, n - 2$), $c_{1,s}^2$, and $c_{1,s}$. Therefore, (B.10) takes the form $\tau P = \tau_v$. As τ is a rectangular matrix, the last row will have two elements when Gaussian elimination is used. Upon multiplication of the matrices and vectors after elimination, the last row becomes a quadratic in $c_{1,s}$. With the selection of a suitable root for $c_{1,s}$ which satisfies $c_{1,s} \geq 0$, the values $c_{j,s}$, $j = 2, n - 2$ can be computed.

Acknowledgements

The authors would like to thank Dr. Jean Riotte for his help with the titration experiments and Indo-French Cell for Water Sciences, IISc-IRD Joint International Laboratory, IISc, Bengaluru for providing the equipment.

References

References

- Al-Abadleh, H. A., Grassian, V., 2003. FT-IR study of water adsorption on aluminum oxide surfaces. *Langmuir* 19, 341–347.
- Appel, C., Rhue, D., Kabengi, N., Harris, W., 2013. Calorimetric investigation of the nature of sulfate and phosphate sorption on amorphous aluminum hydroxide. *Soil Sci.* 178, 180–188.
- Bachet, M., Jauberty, L., De Windt, L., Tevissen, E., De Dieuleveult, C., Schneider, H., 2014. Comparison of mass transfer coefficient approach and Nernst–Planck formulation in the reactive transport modeling of Co, Ni, and Ag removal by mixed-bed ion-exchange resins. *Ind. Eng. Chem. Res.* 53, 11096–11106.
- Benjamin, M. M., 2002. *Water Chemistry*. McGraw-Hill, New York.
- Bird, R. B., Stewart, W. E., Lightfoot, E. N., 2002. *Transport phenomena*. John Wiley & Sons.
- Bockris, J., Reddy, A., Gamboa-Aldeco, M., 2006. *Modern Electrochemistry 2A: Fundamentals of Electrodics*. Springer International edition.

- Carrier, X., Marceau, E., Lambert, J.-F., Che, M., 2007. Transformations of γ -alumina in aqueous suspensions: 1. alumina chemical weathering studied as a function of pH. *J. Colloid Interf. Sci.* 308, 429–437.
- Charmas, R., Piasecki, W., Rudzinski, W., 1995. Four layer complexation model for ion adsorption at electrolyte/oxide interface: Theoretical foundations. *Langmuir* 11, 3199–3210.
- Chatterjee, S., De, S., 2014. Adsorptive removal of fluoride by activated alumina doped cellulose acetate phthalate (CAP) mixed matrix membrane. *Sep. Purif. Technol.* 125, 223–238.
- Curtiss, C., Bird, R. B., 1999. Multicomponent diffusion. *Ind. Eng. Chem. Res.* 38, 2515–2522.
- Cussler, E. L., 2009. *Diffusion: Mass Transfer in Fluid Systems*. Cambridge University Press.
- Davis, J. A., James, R. O., Leckie, J. O., 1978. Surface ionization and complexation at the oxide/water interface: I. Computation of electrical double layer properties in simple electrolytes. *J. Colloid Interface Sci.* 63, 480–499.
- Dou, X., Zhang, Y., Wang, H., Wang, T., Wang, Y., 2011. Performance of granular zirconium–iron oxide in the removal of fluoride from drinking water. *Water Res.* 45, 3571–3578.
- Eaton, A. D., Clesceri, L. S., Rice, E. W., Greenberg, A. E., 2005. *Standard Methods for the Examination of Water and Wastewater*. American Public Health Association (APHA), Washington, DC, USA.
- Fletcher, H., Smith, D., Pivonka, P., 2006. Modeling the sorption of fluoride onto alumina. *J. Environ. Eng.-ASCE* 132, 229–246.
- Frey, D. D., 1986. Prediction of liquid-phase mass-transfer coefficients in multicomponent ion exchange: comparison of matrix, film-model, and effective-diffusivity methods. *Chem. Eng. Commun.* 47, 273–293.
- George, S., Pandit, P., Gupta, A., 2010. Residual aluminium in water de-fluoridated using activated alumina adsorption–modeling and simulation studies. *Water Res.* 44, 3055–3064.

- Gleuckauf, E., 1955. Theory of chromatography part 10: Formula for diffusion into spheres and their applications in chromatography. *T. Faraday Soc.* 51, 1540–1551.
- Goswami, A., Purkait, M. K., 2012. The defluoridation of water by acidic alumina. *Chem. Eng. Res. Des.* 90, 2316 – 2324.
- Gu, W., Wang, C., Liaw, B., 1997. Numerical modeling of coupled electrochemical and transport processes in lead-acid batteries. *J. Electrochem. Soc.* 144, 2053–2061.
- Hao, O. J., Huang, C., 1986. Adsorption characteristics of fluoride onto hydrous alumina. *J. Environ. Eng. ASCE* 112, 1054–1069.
- Islam, M., Patel, R., 2007. Evaluation of removal efficiency of fluoride from aqueous solution using quick lime. *J. Hazard. Mater.* 143, 303–310.
- Jia, Y., Foutch, G. L., 2004. True multi-component mixed-bed ion-exchange modeling. *React. Funct. Polym.* 60, 121–135.
- Jin, X., Qian, Z., Lu, B., Yang, W., Bi, S., 2010. Density functional theory study on aqueous aluminum-fluoride complexes: Exploration of the intrinsic relationship between water-exchange rate constants and structural parameters for monomer aluminum complexes. *Environ. Sci. Technol.* 45, 288–293.
- Kanwar, L., 2010. Defluoridation of drinking water using activated alumina. Master’s thesis, Indian Institute of Science.
- Krishna, R., 1987. Diffusion in multicomponent electrolyte systems. *Chem. Eng. J.* 35, 19–24.
- Krishna, R., Wesselingh, J., 1997. The Maxwell–Stefan approach to mass transfer. *Chem. Eng. Sci.* 52, 861–911.
- Lefevre, G., Duc, M., Lepeut, P., Caplain, R., Fédoroff, M., 2002. Hydration of γ -alumina in water and its effects on surface reactivity. *Langmuir* 18, 7530–7537.
- Liaw, C., Wang, J., Greenkorn, R., Chao, K., 1979. Kinetics of fixed-bed adsorption: A new solution. *AIChE J.* 25, 376–381.

- Mondal, P., George, S., 2015. A review on adsorbents used for defluoridation of drinking water. *Rev. Environ. Sci. Biotechnol.* 14, 195–210.
- Moreira, R., Soares, J., Casarin, G., Rodrigues, A., 2006. Adsorption of CO₂ on Hydrotalcite-like compounds in a fixed bed. *Separ. Sci. Technol.* 41, 341–357.
- Nagashima, K., Blum, F. D., 1999. Proton adsorption onto alumina: Extension of multisite complexation (MUSIC) theory. *J. Colloid Interf. Sci.* 217, 28–36.
- Newman, J., Thomas-Alyea, K. E., 2012. *Electrochemical systems*. John Wiley & Sons, New Jersey.
- Nigussie, W., Zewge, F., Chandravanshi, B., 2007. Removal of excess fluoride from water using waste residue from alum manufacturing process. *J. Hazard. Mater.* 147, 954 – 963.
- Nordin, J. P., Sullivan, D. J., Phillips, B. L., Casey, W. H., 1999. Mechanisms for fluoride-promoted dissolution of bayerite [β -Al(OH)₃ (s)] and boehmite [γ -AlOOH]: ¹⁹F-NMR spectroscopy and aqueous surface chemistry. *Geochim. Cosmochim. Acta* 63, 3513–3524.
- Okamoto, Y., Imanaka, T., 1988. Interaction chemistry between molybdena and alumina: Infrared studies of surface hydroxyl groups and adsorbed carbon dioxide on aluminas modified with molybdate, sulfate, or fluorine anions. *J. Phys. Chem.* 92, 7102–7112.
- Ruthven, D. M., 1984. *Principles of Adsorption and Adsorption Processes*. John Wiley & Sons.
- Ryazanov, M., Dudkin, B., 2003. Acid–base properties of γ -Al₂O₃ suspension studied by pK spectroscopy. *Colloid J+* 65, 761–766.
- Ryazanov, M., Dudkin, B., 2004. The pK spectroscopy study of the acid–base properties of hydrated aluminum oxide sols. *Colloid J+* 66, 726–728.
- Seader, J. D., Henley, E. J., 2006. *Separation process principles*. Wiley India.
- Sircar, S., Hufton, J., 2000. Why does the linear driving force model for adsorption kinetics work? *Adsorption* 6, 137–147.

- Snedecor, G. W., Cochran, W. G., 1968. Statistical Methods. Oxford and IBH Publishing Co.
- Su, C., Suarez, D., 1997. In situ infrared speciation of adsorbed carbonate on aluminum and iron oxides. *Clays Clay Miner.* 45, 814 – 825.
- Tang, Y., Guan, X., Su, T., Gao, N., Wang, J., 2009. Fluoride adsorption onto activated alumina: Modeling the effects of pH and some competing ions. *Colloid. Surface. A* 337, 33–38.
- Tefera, D. T., Hashisho, Z., Philips, J. H., Anderson, J. E., Nichols, M., 2014. Modeling competitive adsorption of mixtures of volatile organic compounds in a fixed-bed of beaded activated carbon. *Environ. Sci. Technol.* 48, 5108–5117.
- Tjaden, B., Cooper, S. J., Brett, D. J., Kramer, D., Shearing, P. R., 2016. On the origin and application of the bruggeman correlation for analysing transport phenomena in electrochemical systems. *Curr. Opin. Chem. Eng.* 12, 44–51.
- Wakao, N., Funazkri, T., 1978. Effect of fluid dispersion coefficients on particle-to-fluid mass transfer coefficients in packed beds: correlation of sherwood numbers. *Chem. Eng. Sci.* 33, 1375–1384.
- Wijnja, H., Schulthess, C., 1999. ATR–FTIR and DRIFT spectroscopy of carbonate species at the aged γ -Al₂O₃/water interface. *Spectrochim. Acta A* 55, 861–872.
- Winkler, B. F., Thodos, G., 1971. Kinetics of orthophosphate removal from aqueous solutions by activated alumina. *J. Water Pollut. Control Fed.* 43, 474–482.